Evidence of cryptic methane cycling and non-methanogenic

2 methylamine consumption in the sulfate-reducing zone of

3 sediment in the Santa Barbara Basin, California

- 4 Sebastian J.E. Krause^{1*#}, Jiarui Liu¹, David J. Yousavich¹, DeMarcus Robinson², David W.
- 5 Hoyt³, Qianhui Qin⁴, Frank Wenzhoefer^{5,6,7}, Felix Janβen^{5,6}, David L. Valentine⁸, and Tina
- 6 Treude^{1,2*}
- ⁷ Department of Earth Planetary and Space Sciences, University of California, Los Angeles, CA
- 8 90095, USA
- ⁹ Department of Atmospheric and Ocean Sciences, University of California, Los Angeles, CA
- 10 90095, USA
- ³Pacific Northwest National Laboratory Environmental and Molecular Sciences Division,
- 12 Richland, WA 99352, USA
- ⁴Interdepartmental Graduate Program in Marine Science, University of California, Santa
- 14 Barbara, CA 93106, USA
- 15 5HGF-MPG Group for Deep-Sea Ecology and Technology, Alfred-Wegener-Institute,
- 16 Helmholtz-Center for Polar and Marine Research, Am Handelshafen 12, 27570 Bremerhaven,
- 17 Germany
- ⁶Max Planck Institute for Marine Microbiology, Celsiusstrasse 1, 28359 Bremen, Germany
- ¹⁹ Department of Biology, DIAS, Nordcee and HADAL Centres, University of Southern
- 20 Denmark, 5230 Odense M, Denmark
- ⁸Department of Earth Science and Marine Science Institute, University of California Santa
- 22 Barbara, Santa Barbara, CA 93106, USA
- *Correspondence: Sebastian Krause (sjkrause@ucsb.edu), Tina Treude (ttreude@g.ucla.edu)

- 24 # Present address: Earth Research Institute, 6832 Ellison Hall, University of California
- 25 Santa Barbara, Ca 93106-3060

Abstract. The recently discovered cryptic methane cycle in the sulfate-reducing zone of marine 26 and wetland sediments couples methylotrophic methanogenesis to anaerobic oxidation of 27 methane (AOM). Here we present evidence of cryptic methane cycling activity within the 28 upper regions of the sulfate-reducing zone, along a depth transect within the Santa Barbara 29 Basin, off the coast of California, USA. The top 0-20 cm of sediment from each station was 30 subjected to geochemical analyses and radiotracer incubations using ³⁵S-SO₄²⁻, ¹⁴C-mono-31 methylamine, and ¹⁴C- CH₄ to find evidence of cryptic methane cycling. Methane 32 concentrations were consistently low (3 to 16 µM) across the depth transect, despite AOM rates 33 increasing with decreasing water depth (from max 0.05 nmol cm⁻³ d⁻¹ at the deepest station to 34 max 1.8 nmol cm⁻³ d⁻¹ at the shallowest station). Porewater sulfate concentrations remained 35 high (23mM to 29 mM), despite the detection of sulfate reduction activity from ³⁵S-SO₄²⁻ 36 incubations with rates up to 134 nmol cm⁻³ d⁻¹. Metabolomic analysis showed that substrates 37 for methanogenesis (i.e., acetate, methanol and methylamines) were mostly below the detection 38 limit in the porewater, but some samples from the 1-2 cm depth section showed non-39 quantifiable evidence of these substrates, indicating their rapid turnover. Estimated 40 methanogenesis from mono-methylamine ranged from 0.2 nmol to 0.5 nmol cm⁻³ d⁻¹. 41 Discrepancies between the rate constants (K₁) of methanogenesis (from ¹⁴C- mono-42 methylamine) and AOM (from either ¹⁴C- mono-methylamine-derived ¹⁴C-CH₄ or from 43 directly injected ¹⁴C-CH₄) suggest the activity of a separate, concurrent metabolic process 44 directly metabolizing mono-methylamine to inorganic carbon. We conclude that the results 45 presented in this work show strong evidence of cryptic methane cycling occurring within the 46 top 20 cm of sediment in the Santa Barbara Basin. The rapid cycling of carbon between 47 methanogenesis and methanotropy likely prevents major build-up of methane in the sulfate-48 reducing zone. Furthermore, our data suggest that methylamine is utilized by both 49 methanogenic archaea capable of methylotrophic methanogenesis and non-methanogenic 50

- 51 microbial groups. We hypothesize that sulfate reduction is responsible for the additional
- 52 methylamine turnover but further investigation is needed to elucidate this metabolic activity.

54 1. Introduction

In anoxic marine sediment, methane is produced by microbial methanogenesis in the 55 last step of organic carbon remineralization (Stephenson and Stickland, 1933; Thauer, 1998; 56 57 Reeburgh, 2007). This methane is produced by groups of obligate anaerobic methanogenic archaea across the Euryarchyota, Crenarchaeota, Halobacterota, and Thermoplasmatota phyla 58 59 (Lyu et al., 2018). Methanogens can produce methane through three different metabolic pathways, using CO₂ (CO₂ reduction; e.g., hydrogenotrophic) (Eq. 1), acetate (acetoclastic) 60 (Eq. 2) and methylated substrates such as, methyl sulfides, methanol, and methylamines 61 (methylotrophic) (e.g., Eq. 3). 62

63
$$4H_2 + CO_2 \rightarrow CH_4 + 2H_2O$$
 [1]

64
$$CH_3COO^- + H^+ \rightarrow CO_2 + CH_4$$
 [2]

65
$$4CH_3NH_2 + 2H_2O \rightarrow 3CH_4 + CO_2 + 4NH_4$$
 [3]

Classically, hydrogenotrophic and acetoclastic methanogenesis are dominant in deeper 66 sulfate-free sediment (Jørgensen, 2000; Reeburgh, 2007). This distinct geochemical zonation 67 is due to the higher free energy gained by sulfate-reducing bacteria within the sulfate reduction 68 zone coupling sulfate reduction with hydrogen and/or acetate consumption in sulfate-rich 69 sediment. Thus, sulfate-reducing bacteria tend to outcompete methanogenic archaea for 70 hydrogen and acetate in shallower sediment layers in the presence of sulfate (Kristjansson et 71 72 al., 1982; Winfrey and Ward, 1983; Lovley and Klug, 1986; Jørgensen, 2000). However, methylotrophic methanogenesis is known to occur within the sulfate-reducing zone. The 73 74 activity of this process in the presence of sulfate reduction is possible because methylated substrates, such as methylamines, are non-competitive carbon sources for methanogens 75 (Oremland and Taylor, 1978; Lovley and Klug, 1986; Maltby et al., 2016; Zhuang et al., 2016; 76 2018; 2018; Krause and Treude, 2021). Methylotrophic methanogenesis activity in the sulfate-77 reducing zone has been detected in a wide range of aquatic environments, such as coastal 78 wetlands (Oremland et al., 1982; Oremland and Polcin, 1982; Krause and Treude, 2021), 79

upwelling regions (Maltby et al., 2016), and eutrophic shelf sediment (Maltby et al., 2018; Xiao et al., 2018). Despite methylotrophic activity in the sulfate-reducing zone, methane concentrations are several orders of magnitude lower than methane concentrations found in deeper sediment zones where sulfate concentrations are depleted (Barnes and Goldberg, 1976; Dale et al., 2008b; Wehrmann et al., 2011; Beulig et al., 2018).

In anoxic marine sediment, anaerobic oxidation of methane (AOM) is an important methane sink that is typically coupled to sulfate reduction (Eq. 4) and mediated by a consortium of anaerobic methane-oxidizing archaea (ANME) and sulfate-reducing bacteria (Knittel and Boetius, 2009; Orphan et al., 2001; Michaelis et al., 2002; Boetius et al., 2000; Hinrichs and Boetius, 2002; Reeburgh, 2007).

90
$$CH_4 + SO_4^{2-} \rightarrow HCO_3^- + HS^- + H_2O$$
 [4]

AOM occurring in the sulfate-reducing zone, fuelled by concurrent methylotrophic methanogenesis activity, i.e., the cryptic methane cycle, could be the reason why methane concentrations are consistently low in sulfidic sediment (Krause and Treude, 2021; Xiao et al., 2017; Xiao et al., 2018). These studies highlight the importance of the cryptic methane cycle on the global methane budget. However, the extent of our knowledge of cryptic methane cycle is restricted to a few aquatic environments. Thus, it is crucial to investigate and understand the cryptic methane cycle in other aquatic environments to fully understand its impact on the global methane budget. In the present study we focus on organic-rich sediment below oxygen-deficient water in the Santa Barbara Basin (SSB), California.

Oxygen minimum zones (OMZ) are regions where high oxygen demand in the water column leads to a dramatic decline or even absence of dissolved oxygen (Wright et al., 2012; Paulmier and Ruiz-Pino, 2009; Wyrtki, 1962; Canfield and Kraft, 2022). In these environments, coastal upwelling of nutrients results in high phytoplankton growth, greatly enhancing organic matter loading and in turn creating a high metabolic oxygen demand during organic matter degradation in the water column. This enhanced respiration depletes oxygen

faster than it is replenished (especially in poorly ventilated water bodies), which results in seasonal or continuous low oxygen conditions (Wyrtki, 1962; Helly and Levin, 2004; Wright et al., 2012; Levin et al., 2009). Sediment beneath OMZs is typically rich in organic matter supporting predominantly or exclusively anaerobic degradation processes, including methanogenesis (Levin, 2003; Rullkötter, 2006; Middelburg and Levin, 2009; Fernandes et al., 2022; Treude, 2011). Thus, sediments underlying OMZ's are good candidate environments to investigate cryptic methane cycling.

Located within the Pacific Ocean, between the Channel Islands and the mainland of Santa Barbara, California, USA, the SBB is characterized as a thermally stratified, coastal marine basin with a maximum water column depth of approximately 590 m (Soutar and Crill, 1977; Arndt et al., 1990; Sholkovitz, 1973). Low oxygen concentrations (<10 μM) are found in the bottom waters below the sill depth (~475 m) of the SBB (Sholkovitz, 1973; Reimers et al., 1996). The sediment in the SBB have an organic carbon content between 2-6% (Schimmelmann and Kastner, 1993). These characteristics make the SBB a prime study site to find evidence of cryptic methane cycling.

Organic carbon sources for methylotrophic methanogenesis, such as methylamine, are ubiquitous in coastal marine environments (Zhuang et al., 2018; Zhuang et al., 2016; Oren, 1990), including marine environments where OMZ's exist (Ferdelman et al., 1997; Gibb et al., 1999). Methylamines are derived from osmolytes, such as glycine and betaine, and are synthesized by phytoplankton (Oren, 1990). However, the abundance of methylamines and how they may be driving cryptic methane cycling in anoxic sediment within OMZ's is virtually unknown. Furthermore, the fate of methane from methylotrophic methanogenesis in the sulfate reduction zone is poorly constrained. Particularly, if cryptic methane cycling is active above the sulfate-methane transition zone, gross production and consumption of methane have likely been underestimated. Therefore, finding evidence for the cryptic methane cycle in the SBB is

a necessary step towards understanding how carbon is cycled through the sediment of the SBB and other OMZs.

In the present study we report biogeochemical evidence of cryptic methane cycling in surface sediment (top \sim 15 cm) collected along a depth transect crossing the SBB. We applied the radiotracer method from Krause and Treude (2021) to trace the production of methane from mono-methylamine, followed by the anaerobic oxidation of methane to inorganic carbon. We combined this approach with standard radiotracer methods for the detection of AOM and sulfate reduction as well as with analyses of sediment porewater geochemistry.

2. Methods.

2.1. Study site and sediment sampling

Sediment samples were collected during the R/V *Atlantis* expedition AT42-19 in fall 2019. Collection was achieved with polycarbonate push cores (30.5 cm long, 6.35 cm i.d.), which were deployed by the ROV *JASON* along a depth transect through the SBB. The depth transect selected for this particular study, was the Northern Deposition Transect 3 (NDT3), with three stations (NDT3-A, -C and -D), as well as the Northern Depositional Radial Origin (NDRO), and the Southern Depositional Radial Origin (SDRO) station, located in the deepest part of the basin. Details on the stations' water column depths and near-seafloor oxygen concentrations are provided in Table 1.

Table 1. Water column depth, bottom water oxygen concentrations and coordinates of each station sampled during this study.

Station	Depth (m)	Bottom Water Oxygen (μΜ)	Latitude	Longitude
SDRO	586	0	34.2011	-120.0446
NDRO	580	0	34.2618	-120.0309
NDT3-A	572	9.2	34.2921	-120.0258
NDT3-C	498	5	34.3526	-120.0160
NDT3-D	447	8	34.3625	-120.0150

After sediment collection, ROV push cores were returned to the surface by an elevator platform. Upon retrieval onboard the R/V *Atlantis*, sediment samples were immediately transported to an onboard cold room (6°C) for further processing of biogeochemical parameters (see details in section 2.2.).

2.2. Sediment porewater sampling and sulfate analysis

For porewater analyses, two ROV sediment push cores from each station were sliced in 1-cm increments in the top 10 cm of the sediment, followed by 2-cm increments below.

During sediment sampling, ultra-pure argon was flushed over the sediment to minimize oxidation of oxygen sensitive species. The sliced sediment layers were quickly transferred to argon-flushed 50 mL plastic centrifuge vials and centrifuged at 2300 X g for 20 mins to extract the porewater. Subsequently, 2 mL of porewater was subsampled from the supernatant and frozen at -20 °C for shore-based sulfate analysis by ion chromatography (Metrohm 761) following (Dale et al., 2015). Additional porewater (1 mL) was subsampled for the determination of the concentration of methylamine and other metabolic substrates (see section 2.4).

2.3. Sediment methane and benthic methane flux analyses

Methane concentration in the sediment was determined from a replicate ROV pushcore. Sediment was sliced at 1-cm increments in the top 10 cm, followed by 2-cm increments below. Two mL of sediment was sampled with a cut-off 3 mL plastic syringe and quickly transferred to 12 mL glass serum vials filled with 5 mL 5% (w/w) NaOH solution. The vials were sealed immediately with a grey butyl rubber stopper and aluminum crimps, shaken thoroughly, and stored upside down at 4 °C. Methane concentrations in the headspace were determined shore-based using a gas chromatograph (Shimadzu GC-2015) equipped with a packed Haysep-D column and flame ionization detector. The column was filled with helium as a carrier gas, flowing at 12 mL per minute and heated to 80 °C. Methane concentrations in the environmental samples were calibrated against methane standards (Scott Specialty Gases) with a \pm 5% precision.

To determine methane flux out of the sediment and into the water column, 1-2 custom-built cylindrical benthic flux chambers (BFC) (Treude et al., 2009) were deployed at each sampling station by the ROV Jason. The BFCs consist of a lightweight fiber-reinforced plastic frame, which holds a cylindrical polycarbonate chamber. Buoyant syntactic foam was attached to the feet of the frame to keep the BFC's from sinking too deep into the soft and

poorly consolidated sediments, especially in the deeper stations. Water overlying the enclosed sediment was kept mixed with a stirrer bar rotating below the lid of the chamber. The BFC's were equipped with a syringe sampler holding seven, 50 mL glass syringes (6 syringes for sample collection and 1 syringe for freshwater injection). One sample syringe withdrew 50 mL of seawater from the chamber volume at pre-programed time intervals. The seventh syringe was used to inject 50 mL of de-ionized water into the chamber shortly after deployment to calculate the volume from the change in salinity in the overlying seawater recorded by a conductivity sensor (type 5860, Aanderaa Data Instruments, Bergen, NO), according to (Kononets et al., 2021).

Seawater samples to determine the methane flux out of the sediments were collected in 26 mL serum glass bottles. The 26 mL serum bottles were acid cleaned, and then combusted at 300 °C prior to BFC seawater sample collection. One to two pellets of solid NaOH were added into each empty 26 mL combusted serum bottle. All empty serum bottles were then flushed with ultra-pure nitrogen gas (Airgas Ultra High Purity Grade Nitrogen, Manufacturer Part #:UHP300) for 5 min, then sealed with autoclaved chlorobutyl stoppers and crimps. Lastly, a vacuum pump was used to evacuate the bottles to a pressure down to <0.05 psi prior to sample collection.

Immediately after BFC recovery from the seafloor, approximately 20 mL of seawater sample was transferred into the pre-evacuated, acid cleaned, and combusted 26 mL glass serum bottles through the chlorobutyl stopper using a sterile 23G needle. Pressure within the serum bottle was equalized to atmospheric pressure with the introduction of UHP grade nitrogen. Serum bottles were shaken to dilute the NaOH pellets, which terminated metabolic activity and forced the dissolved methane into the gas headspace. The serum bottles were reweighed after sample collection, to calculate the exact volume of the seawater sample. Methane concentrations in seawater collected from the BFC's were analyzed shipboard by gas chromatography according to Qin et al., 2022.

Total methane concentration in the headspace was calculated following the ideal gas law Eq. (5),

215
$$n = \frac{PV}{RT} * [CH_4] * \frac{1}{V_{SW}}$$
 [5]

Where n is the total molar concentration of methane, P is atmospheric pressure, V is the volume of the headspace of serum bottle (which is calculated by 26 mL subtracted by the volume of seawater sample), R is the ideal gas constant, T is temperature in Kelvin (288.15 K), $[CH_4]$ is the methane measured by GC as percentage values in ppm, and V_{SW} is the volume of seawater in the serum vial. The volume of sampled seawater in each serum bottle was calculated by subtracting the mass of the empty serum bottle from the mass of the filled serum bottle, normalized by the density of seawater.

223

224

2.4. Determination of methanogenic substrates in porewater

225 To sediment porewater concentrations of methanogenic 226 (methylamine, methanol, and acetate), 1 mL porewater was extracted from 1-2 cm and 9-10 227 cm depth sections at each station (see section 2.2) and syringe-filtered (0.2 µm) into precombusted (350 °C for 3 hrs) amber glass vials (1.8 mL), which were then closed with a PTFE 228 septa-equipped screw caps and frozen at -80 °C until analyses. Samples were analysed at the 229 Pacific Northwest National Laboratory, Environment and Molecular Sciences Division for 230 231 metabolomic analysis using proton nuclear magnetic resonance (NMR). Prior to analysis, porewater samples were diluted by 10% (v/v) with an internal standard (5 mM 2.2-dimethyl-232 233 2-silapentane-5-sulfonate-d6). All NMR spectra were collected using an 800 MHz Bruker Avance Neo (Tava), with a TCl 800/54 H&F/C/N-D-05 Z XT, and an QCl H-P/C/N-D-05 Z 234 ET extended temperature range CryoProbe. The 1D 1H NMR spectra of all samples were 235 processed, assigned, and analysed by using the Chenomx NMR Suite 8.6 software with 236 quantification based on spectral intensities relative to the internal standard. Candidate 237 metabolites present in each of the complex mixture were determined by matching the chemical 238

shift, J-coupling, and intensity information of experimental NMR signals against the NMR signals of standard metabolites in the Chenomx library. The 1D 1H spectra were collected following standard Chenomx data collection guidelines, employing a 1D NOESY presaturation experiment (noesypr1d) with 65536 complex points and at least 4096 scans at 298 K. Signal to noise ratios (S/N) were measured using MestReNova 14 with the limit of quantification equal to a S/N of 10 and the limit of detection equal to a S/N of 3. The 90° ¹H pulse was calibrated prior to the measurement of each sample with a spectral width of 12 ppm and 1024 transients. The NOESY mixing time was 100 ms and the acquisition time was 4 s followed by a relaxation delay of 1.5 s during which presaturation of the water signal was applied. Time domain free induction decays (72114 total points) were zero-filled to 131072 total points prior to Fourier transform.

2.53

2.54

2.5. Metabolic activity determinations

One replicate ROV sediment push core (hereafter 'ROV rate push core') from each station was sub-sampled with three mini-cores (20 cm long, 2.6 cm i.d.) for radiotracer incubations according to the whole-core injection method (Jørgensen 1978) to collect quantitative metabolic evidence (sulfate reduction, methanogenesis, methane oxidation) of cryptic methane cycling. The incubation methods are detailed below. Note that not enough sediment cores were collected at each station to perform replicate radiotracer experiments that would have allowed addressing small-scale spatial variability in ex-situ rates.

2.5.1. Sulfate reduction via ³⁵S-Sulfate

Within the same day of collection, one mini-core from each ROV rate push core was used to determine sulfate-reduction rates. Radioactive carrier-free ³⁵S-sulfate (³⁵S-SO₄²⁻; dissolved in MilliQ water, injection volume 10 μL, activity 260 KBq, specific activity 1.59 TBq mg⁻¹) was injected into the mini core at 1-cm increments and incubated at 6 °C in the dark

following (Jørgensen, 1978). Injected sediment cores were stored vertically and incubated for ~6 hrs at 6 °C in the dark. Incubations were stopped by slicing the sediment in 1-cm increments into 50 mL plastic centrifuge tubes containing 20 mL 20% (w/w) zinc acetate solution. Each sediment sample was sealed and shaken thoroughly and stored at -20 °C to halt metabolic activity. For the control samples, sediments were added to zinc acetate solution prior to radiotracer injection. In the home laboratory, sulfate reduction rates were determined using the cold-chromium distillation method (Kallmeyer et al., (2004).

2.5.2. Methanogenesis and AOM via ¹⁴C-Mono-Methylamine

This study aimed at determining the activity of methanogenesis from monomethylamine (MG-MMA) and the subsequent anaerobic oxidation of the resulting methane to inorganic carbon by AOM (AOM-MMA). To accomplish this goal, a mini core from each ROV rate push core was injected with radiolabeled ¹⁴C-mono-methylamine (¹⁴C-MMA; dissolved in 1 mL water, injection volume 10 µL, activity 220 KBq, specific activity 1.85-2.22 GBq mmol⁻¹) similar to section 2.5.1. After 24 hrs, the incubation was terminated by slicing the sediment at 1-cm increments into 50 mL wide mouth glass vials filled with 20 mL of 5% NaOH. Five killed control samples were prepared by transferring approximately 5 ml of extra sediment from each station into 50 mL wide mouth vials filled with 20 mL of 5% NaOH prior to radiotracer addition. Sample vials and vials with killed controls were immediately sealed with butyl rubber stoppers and aluminium crimps and shaken thoroughly for 1 min to ensure complete biological inactivity. Vials were stored upside down at room temperature until further processing. In the home laboratory, methane production from ¹⁴C-MMA by MG-MMA and subsequent oxidation of the produced ¹⁴C-methane (¹⁴C-CH₄) by AOM-MMA was determined according to the adapted radiotracer method outlined in (Krause and Treude, 2021).

To account for ¹⁴C-MMA potentially bound to mineral surfaces (Wang and Lee, 1993, 1994; Xiao et al., 2022), we determined the ¹⁴C-MMA recovery factor (RF) for the sediment from the stations NDT3-C, D and NDRO according to Krause and Treude (2021).

Metabolic rates of MG-MMA were calculated according to Eq. 7. Note that natural concentrations of MMA in the SBB sediment porewater were either below detection or detectable, but below the quantification limit ($<10~\mu\text{M}$) (Table S1). Therefore, MMA concentrations were assumed to be 3 μM to calculate the ex-situ rate of MG-MMA (Eq. 8).

296
$$MG\text{-}MMA = \frac{a_{CH_4} + a_{TIC}}{a_{CH_4} + a_{TIC} + \left[\frac{a_{MMA}}{RF}\right]} * [MMA] * \frac{1}{t}$$
 [7]

where MG-MMA is the rate of methanogenesis from mono-methylamine (nmol cm⁻³ d⁻¹); a_{CH4} is the radioactive methane produced from methanogenesis (CPM); a_{TIC} is the radioactive total inorganic carbon produced from the oxidation of methane (CPM); a_{MMA} the residual radioactive mono-methylamine (CPM); RF is the recovery factor (Krause and Treude, (2021); [MMA] is the assumed mono-methylamine concentrations in the sediment (nmol cm⁻³); t is the incubation time (d). ¹⁴C-CH₄ and ¹⁴C-TIC sample activity was corrected by respective abiotic activity determined in killed controls.

Results from the ¹⁴C-MMA incubations were also used to estimate the AOM-MMA rates according to Eq. 8,

306
$$AOM\text{-}MMA = \frac{a_{TIC}}{a_{CH_4} + a_{TIC}} * [CH_4] * \frac{1}{t}$$
 [8]

where AOM-MMA is the rate of anaerobic oxidation of methane based on methane produced from MMA (nmol cm⁻³d⁻¹); a_{TIC} is the produced radioactive total inorganic carbon (CPM); a_{CH4} is the residual radioactive methane (CPM); $[CH_4]$ is the sediment methane concentration (nmol cm⁻³); t is the incubation time (d). ¹⁴C-TIC activity was corrected by abiotic activity determined by replicate dead controls.

312

313

292

293

294

295

2.5.3 Anaerobic oxidation of methane via ¹⁴C-Methane

AOM rates from ¹⁴C-CH₄ (AOM-CH₄) were determined by injecting radiolabeled ¹⁴C-CH₄ (dissolved in anoxic MilliQ, injection volume 10 μL, activity 5 KBq, specific activity 1.85–2.22 GBq mmol⁻¹) into one mini core from each ROV rate core at 1-cm increments similar to section 2.5.1. Incubations of the mini cores were stopped after ~24 hours similar to section 2.5.2. In the laboratory, AOM-CH₄ was analysed using oven combustion (Treude et al., 2005) and acidification/shaking (Joye et al., 2004). The radioactivity was determined by liquid scintillation counting. AOM-CH₄ rates were calculated according to Eq. 8.

321

322 2.5.4 Rate constants for AOM-CH₄, MG-MMA, and AOM-MMA

323

- Metabolic rate constants (k) for AOM-CH4, MG-MMA and AOM-MMA were calculated for relative turnover comparisons using the experimental data determined by sections 2.5.2 and
- 326 2.5.3. The rate constants consider the metabolic reaction products, divided by the sum of
- reaction reactants and products and by time. The metabolic rate constants for AOM-CH₄, MG-
- 328 MMA and AOM-MMA were calculated according to Eq. 9,

$$329 \quad k = \frac{a_{products}}{a_{products} + a_{reactants}} * \frac{1}{t}$$
 [9]

330 where k is the metabolic rate constant (day⁻¹); $a_{products}$ is the radioactivity (CPM) of the

metabolic reaction products; $a_{reactants}$ is the radioactivity (CPM) of the metabolic reaction

332 reactants; t is time in days.

3. Results

3.1. Sediment biogeochemistry

At most stations, porewater methane concentrations in the top 10-20 cm of sediment fluctuated between 3 and 13 μ M with no clear trend (Fig. 1A, E, I, M, and Q). At NDRO, methane steadily increased below 12 cm, reaching 16 μ M at 14–15 cm (Fig. 1E). Methane concentrations determined in water samples from the BFC incubations revealed only minor fluctuations over time with no clear trends, suggesting no net fluxes of methane into or out of the sediment at all stations (Fig.1S). It is notable, however, that the BFCs captured higher methane concentrations (350-800 nM) in the supernatant of station SDRO, NDRO, and NDT3-A compared to NDT3-C and NDT3-D (< 130 nM). Sulfate concentrations showed no strong decline with depth at any station (except maybe a weak tendency at SDRO and NDT3-A) and fluctuated between 23 and 30 mM in the sampled top 10-20 cm (Fig. 1A, E, I, M, and O).

Table S1 provides porewater concentrations of organic carbon sources from the metabolomic analysis, as measured by NMR, that are known to support methanogenesis. Methylamine was detected at SDRO and NDT3-A (1–2 cm), but those concentrations were below the quantification limit (10 μ M). Otherwise, methylamine was below detection (<3 μ M) for all other samples. Similarly, methanol was detected but below quantification at NDT3-A (1–2 cm) but otherwise below detection. Acetate was at a quantifiable level (21 μ M) at NDT3-A (1–2 cm) but was otherwise either below quantification (SDRO, 1-2 cm; NDRO, 1-2 cm) or below detection.

3.2 AOM from ¹⁴C-methane and sulfate reduction from ³⁵S-sulfate

Fig. 1B, F, J, N, and R depict ex-situ rates of AOM-CH₄ and sulfate reduction from the radiotracer incubations with ¹⁴C-methane and ³⁵S-sulfate in sediment mini cores, respectively. AOM-CH₄ activity tended to increase with decreasing water depth in the top 5 cm of the sediment (from max 0.05 nmol cm⁻³ d⁻¹ at NDRO to max 4.5 nmol cm⁻³ d⁻¹ at NDT3-D), while

rates were either negligible (SDRO, NDRO, NDT3-A) or <1 nmol cm⁻³ d⁻¹ (NDT3-C, NDT3-D) for depths >5 cm. Where peaks in AOM were present (SDRO, NDT3-C, NDT3-D) they were always located in the top 0–1 cm sediment layer.

Sulfate reduction activity was detected throughout all sediment cores with the highest rates mostly at 0–1 cm, followed by a decrease with increasing sediment depth. The highest individual sulfate reduction peaks were found at NDRO, NDT3-A, and NDT3-C (120, 85 and 133 nmol cm⁻³ d⁻¹). At NDT3-D sulfate reduction rates varied between 14 and 45 nmol cm⁻³ d⁻¹ throughout the core with no clear trend. Note that sulfate reduction data are missing for 0–5 cm at SDRO, due to post-cruise analytical issues. Here, rates gradually decreased from 52 to 10 nmol cm⁻³ d⁻¹ below 5 cm.

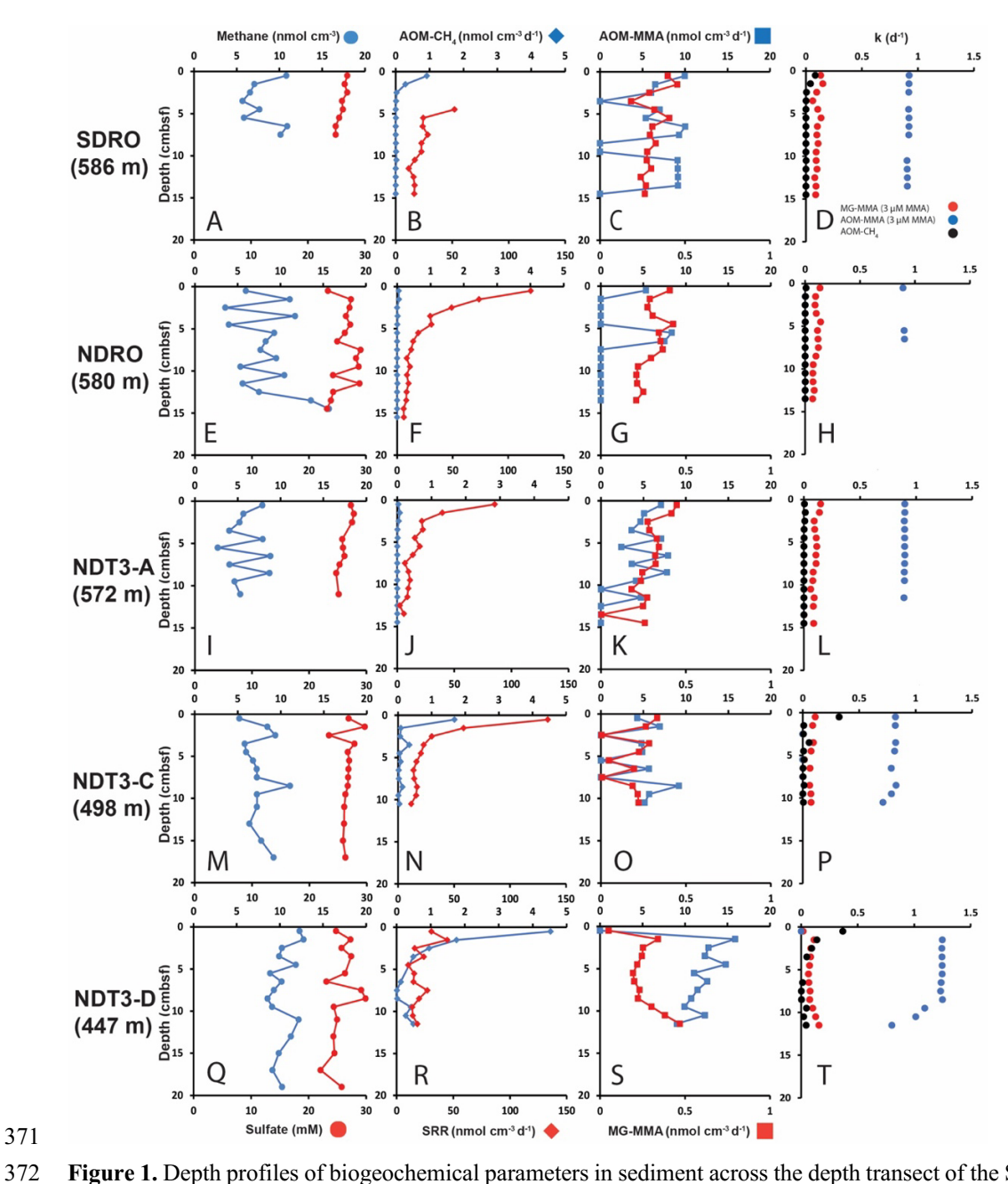


Figure 1. Depth profiles of biogeochemical parameters in sediment across the depth transect of the Santa Barbara Basin. A, E, I, M, and Q: sediment methane and porewater sulfate; B, F, J, N, and R: AOM-CH₄ and sulfate reduction (determined from direct injection of ¹⁴C-CH₄ and ³⁵S-Sulfate, respectively); C, G, K, O, and S: AOM-MMA and MG-MMA (determined from direct injection of ¹⁴C-MMA); D, H, L, P, and T: rate constants for AOM-CH₄, MG-MMA and AOM-MMA.

3.3 Methanogenesis and AOM from ¹⁴C-mono-methylamine

378 3.3.1 ¹⁴C-MMA recovery from sediment

- 379 RF values determined in sediments from NDRO, NDT3-C and D stations (see section
- 380 2.5.2) were 0.93, 0.84, and 0.75, respectively. They were used to correct MG-MMA rates at
- each station of the study. Note that no RF values were determined for SDRO or the NDT3-A.
- We applied RF values from NDRO and NDT3-C, respectively, instead.

383

384

3.3.2 MG-MMA and AOM-MMA

- Fig. 1C, G, K, O, S show ex-situ rates of MG-MMA and AOM-MMA, assuming a
- natural MMA concentration of 3 µM (see section 2.5.2). At SDRO, NDRO, and NDT3-A, MG-
- 387 MMA ranged between 0.27 and 0.45 nmol cm⁻³ d⁻¹ throughout the sediment core without trend
- 388 (Fig. 1C, G, and K). At NDT3-C MG-MMA ex-situ rates were lower ranging between 0.007
- nmol cm⁻³ d⁻¹ and 0.3 nmol cm⁻³ d⁻¹ without any pattern (Fig. 10). At NDT3-D, MG-MMA
- sharply increased from 0.05 nmol cm⁻³ d⁻¹ at 0–1cm, to ~0.34 nmol cm⁻³ d⁻¹ at 1–2 cm. MG-
- 391 MMA then decreased slightly to ~0.2 nmol cm⁻³ d⁻¹ between 2 and 9 cm, before increasing to
- $\sim 0.5 \text{ nmol cm}^{-3} \text{ d}^{-1}$ at the bottom of the core (Fig. 1S).
- AOM-MMA rates were 1 to 2 orders of magnitude higher than MG-MMA rates and 1
- to 4 orders of magnitude higher than AOM-CH₄ rates (Fig 1C, G, K, O, S). At SDRO, NDRO,
- NDT3-A, and NDT3-C, AOM-MMA ex-situ rates ranged between 5.3 and 10 nmol cm⁻³ d⁻¹
- 396 (unless zero) with no trend (Fig 1C, G, K, and O). At NDT3-D, AOM-MMA rates decreased
- 397 from 15.9 nmol cm⁻³ d⁻¹ at 1–2 cm to 9 nmol cm⁻³ d⁻¹ at 11–12 cm (Fig. 1S). At all stations,
- 398 some sediment intervals showed no biological net AOM-MMA activity (Fig 1C, G, K, O, S).
- 399 In these sediment intervals, the ¹⁴C-TIC activity was statistically not different from the average
- 400 plus the standard deviation of the killed control samples.

401

402

3.4 Rate constants for MG-MMA, AOM-MMA and AOM-CH4

Fig. 1D, H, L, P, and T show the rate constants (k) for MG-MMA, AOM-MMA and AOM-CH₄ for the comparison of relative radiotracer turnover. At all stations, MG-MMA rate constants were between 0.01 and 0.15 d⁻¹. AOM-CH₄ rate constants ranged between 0.0009 d⁻¹ and 0.3 d⁻¹. Rate constants for AOM-MMA, however, were considerably higher than MG-MMA and AOM-CH₄ with values ranging between 0.7 and 1.2 d⁻¹. Most rate constants remained constant over depth, with the exemption of AOM-MMA at station NDT3-C and D (Fig. 1P and T), which showed a steady decrease below 9 cm.

4. Discussion

411412

413

414

415

416

417

418

419

420

421

422

423

424

425

426

427

428

429

430

431

432

433

434

435

410

4.1. Evidence of cryptic methane cycling

The aim of the present study was to check for the existence of cryptic methane cycling in SBB surface sediments by presenting evidence for the concurrent activity of sulfate reduction, AOM, and methanogenesis through radiotracer incubations (35S -SO₄-2, 14C-CH₄, and ¹⁴C-MMA, respectively). Our study confirmed indeed that the three processes co-exist at all investigated stations (Fig. 1). The most prominent concurrent metabolic activity was evident from activity peaks near the sediment-water interface at station NDT3-C (Fig. 1N and O). We suggest the concurrent peaking was stimulated by the availability of fresh, i.e., recently deposited, organic matter coinciding with low oxygen concentrations in the bottom water (Table 1). Fresh organic material likely provided a source for both organical satisfactory reduction and methylotrophic methanogenesis, and indirectly (i.e., linked to the methane produced) for AOM coupled to either nitrate, iron, or sulfate reduction. Low oxygen concentrations offered favourable conditions for anaerobic processes in the surface sediment. At the remaining stations (SDRO, NDRO, SDT3-A, SDT3-D; Fig. 1), metabolic activity of all three processes was also confirmed near the sediment surface (with the exemption of the missing data for sulfate reduction at SDRO), but they not always depicted rate peaks (particularly not for AOM-CH₄).

Methane detected in the sulfate-rich sediment (Fig. 1A, E, I, M, Q) was likely produced by methylotrophic methanogenesis utilizing non-competitive substrates within the sulfate-reducing zone (Oremland and Taylor, 1978; King et al., 1983; Maltby et al., 2016; Maltby et al., 2018; Reeburgh, 2007), which is also indicated by the production of methane from our 14 C-MMA incubations. It is interesting to note that methane concentrations remained relatively constant around 5 to 12 μ M while AOM-CH₄ tended to increase with decreasing water depth. This pattern suggests that the partial pressure of methane was likely determined by

thermodynamic equilibrium between methanogenesis and AOM (compare, e.g., with Conrad 1999).

The finding of non-linear methane concentrations in surface sediments is against the general view that methane concentrations above the sulfate-methane transition zone show a linear, diffusion-controlled decline towards the sediment-water interface, where methane escapes into the water column (Reeburgh, 2007). We argue that the non-linear methane trends we observe in the present study is an indication for simultaneous methane production and consumption, i.e., cryptic methane cycling, as evident from our radiotracer experiments.

As there is considerable methanogenic activity even at the sediment-water interface (0-1 cm) at all stations, aside from station NDT3-D (Fig. 1C, G, K, O, S), it is conceivable that some methane could diffuse into the water column where it may be oxidized by either aerobic or anaerobic oxidation processes (depending on the presence or absence of oxygen, respectively) before emission into the atmosphere (Reeburgh, 2007). However, benthic chamber incubations at the SBB stations did not indicate a release of methane into the water column (Fig. S1), emphasizing the importance of cryptic methane cycling for preventing the build-up of methane in the surface sediment and its emission into the water column.

4.2. Rapid turnover of metabolic substrates

Natural porewater MMA concentrations were mostly below detection (<3 μ M); however, in porewater close to the sediment-water interface of SDRO and NDT3-A, MMA was detected but below the quantification limit (<10 μ M) (Table S1). Although we are unable to report definitive MMA concentrations, we can bracket the MMA concentrations in a range between 3 and 10 μ M. The bracketed MMA concentrations are about 1 to 2 orders of magnitude higher than what has been reported from porewater at other locations. For example, studies of sediment porewater off the coast of Peru found MMA concentrations to be ~0.15 μ M (Wang and Lee, 1990). Similarly, in sediment porewater collected from Buzzards Bay, Massachusetts

and in the Eastern Tropical North Pacific Ocean, MMA concentrations were either present at trace amounts or below detection limit (<0.05 μM) (Lee and Olson, 1984). Detectable but low methylamine concentrations in the porewater found in our study could imply that methylamines are rapidly consumed by microbiological processes and/or removed from the porewater through binding to minerals (Wang and Lee, 1990; Wang and Lee, 1993; Xiao et al., 2022). Our study provided support for both hypotheses as we detected the biological potential for MMA consumption via radiotracer (¹⁴C-MMA) experiments (Fig. 1) and detected the binding of 7-25% the injected ¹⁴C-MMA to sediment (see 3.3.1).

Porewater methanol concentrations in the present study were also mainly below detection, except for one sample, where it was not quantifiable (NDT3-A, 1–2 cm; Table S1). In the marine environment, methanol is known to be a non-competitive substrate for methanogenesis (King et al., 1983; Oremland and Taylor, 1978). However, a recent study demonstrated that methanol is a carbon source for a wide variety of metabolisms, including sulfate-reducing and denitrifying bacteria, as well as aerobic and anaerobic methylotrophs (Fischer et al., 2021), which could all be present in the SBB sediments keeping methanol concentrations low. Acetate was also detected in the metabolomic analysis but mostly below quantification (except NDT3-A, 1–2 cm; Table S1). Acetate is formed through fermentation reactions or through homoacetogenesis (Jørgensen, 2000; Ragsdale and Pierce, 2008). It is a favourable food source for many bacteria and archaea such as sulfate reducers and methanogens (Jørgensen, 2000; Conrad, 2020), which would explain its low concentration in the SBB sediments. Low concentrations of the abovementioned metabolites are likely signatures of rapid metabolic turnover, similar to what has been described for microbial utilization of hydrogen in sediment (Conrad, 1999; Hoehler et al., 2001). In this situation, metabolites would be kept at a steady-state concentration close to the thermodynamic equilibrium of the respective consumers.

462

463

464

465

466

467

468

469

470

471

472

473

474

475

476

477

478

479

480

481

482

483

484

4.3. Competitive methylamine turnover by non-methanogenic pathways

Large disparities were found between AOM rates determined from the direct injection of ¹⁴C-CH₄ (i.e., AOM-CH₄) and AOM determined from the production of ¹⁴C-TIC in the ¹⁴C-MMA incubations (i.e., AOM-MMA). AOM-CH₄ was roughly 1-2 orders of magnitude lower compared to AOM-MMA (compare Fig. 1 B/C, F/G, J/K, N/O, R/S), indicating that AOM rates determined via ¹⁴C-MMA incubations were overestimated. We hypothesize that this disparity is the result of the direct conversion of ¹⁴C-MMA to ¹⁴C-TIC by processes other than AOM coupled to MG-MMA. Any process converting ¹⁴C-MMA directly to ¹⁴C-TIC would inflate the rate constant only slightly for MG-MMA, but dramatically for AOM-MMA (see Eq. 8, 9, and 10). Fig. 1D, H, L, P, and T confirm that the rate constants for AOM-MMA are 1 to 2 orders of magnitude higher compared to AOM-CH₄ and MG-MMA. We interpret the difference in these rate constants to strongly suggests that the ¹⁴C-TIC detected in the analysis of samples incubated with ¹⁴C-MMA must result not only from AOM involved in the cryptic methane cycle but also from direct methylamine oxidation by a different anaerobic methylotrophic metabolism that could not be disambiguated using the adapted radiotracer method.

Methylamines are the simplest alkylated amine. They are derived from the degradation of choline and betaine found in plant and phytoplankton biomass (Oren, 1990; Taubert et al., 2017). The molecules are ubiquitously found in saline and hypersaline conditions in the marine environment (Zhuang et al., 2016; Zhuang et al., 2017; Mausz and Chen, 2019). The importance of methylamine as a nitrogen and carbon source for microbes to build biomass has been well documented (Taubert et al., 2017; Capone et al., 2008; Anthony, 1975; Mausz and Chen, 2019). Methylamines can be metabolized by aerobic methylotrophic bacteria (Taubert et al., 2017; Chistoserdova, 2015; Hanson and Hanson, 1996) and by methylotrophic methanogens anaerobically (Chistoserdova, 2015; Thauer, 1998). Based on the data reported

in the present study, we suggest that, in addition to methylotrophic methanogenesis, sulfate reduction was involved in MMA consumption in surface sediment of the SBB.

52.7

Recent literature does implicate anaerobic methylamine oxidation by sulfate reduction. For example, Cadena et al. (2018) performed in vitro incubations with microbial mats collected from a hypersaline environment with various competitive and non-competitive substrates including tri-methylamine. Microbial mats incubated with trimethylamine stimulated considerable methane production; but after 20 days, H₂S began to accumulate and plateaued after 40 days, suggesting that trimethylamine is not exclusively shuttled to methylotrophic methanogenesis. The molecular data reported in Cadena et al. (2018), however, could not identify a particular group of sulfate-reducing bacteria that proliferated by the addition of trimethylamine. Instead, their molecular data suggested potentially other, non-sulfate reducing bacteria, such as those in the family *Flavobacteriaceae* to be responsible for trimethylamine turnover.

Zhuang et al., (2019) investigated heterotrophic metabolisms of C1 and C2 low molecular weight compounds in anoxic sediment collected in the Gulf of Mexico. Sediment was incubated with a variety of ¹⁴C radiotracers alone and in combination with molybdate, a known sulfate reducer inhibitor, to elucidate the metabolic turnover of low molecular weight compounds, including ¹⁴C-labeled trimethylamine. Their results showed that although methylamines did stimulate methane production, radiotracer incubations with molybdate and methylamine demonstrated the inhibition of direct oxidation of ¹⁴C-methylamine to ¹⁴C-CO₂, suggesting that methylamines were simultaneously oxidized to inorganic carbon by nonmethanogenic microorganisms. This finding further suggests a competition between methanogens and sulfate-reducing bacteria for methylamine; however, the authors could not rule out AOM as a potential contributor to the inorganic carbon pool.

Kivenson et al., (2021) discovered dual genetic code expansion in sulfate-reducing bacteria from sediment within a deep-sea industrial waste dumpsite in the San Pedro Basin,

California, which potentially allows the metabolization of trimethylamine. The authors expanded their study to revisit metagenomic and metatranscriptomic data collected from the Baltic Sea and in the Columbia River Estuary and found expression of trimethylamine methyltransferase in Deltaproteobacteria. This result suggested that a trimethylamine metabolism does exist in sulfate-reducing bacteria which was enabled by the utilization of genetic code expansion. Furthermore, the results also suggest that trimethylamine could be the subject of competition between sulfate-reducing bacteria and methylotrophic methanogens.

Although the evidence of sulfate-reducing bacteria playing a larger role in methylamine utilization is growing, there are other methylotrophic microorganisms in anaerobic settings that could also be responsible for degrading methylamines. De Anda et al. (2021) discovered and classified a new phylum called Brockarchaeota. The study reconstructed archaeal metagenome-assembled genomes from sediment near hydrothermal vent systems in the Guaymas Basin, Gulf of California, Mexico. Their findings showed that some Brockarchaeota are capable of assimilating trimethylamines, by way of the tetrahydrofolate methyl branch of the Wood-Ljungdahl pathway and the reductive glycine pathway, bypassing methane production in anoxic sediment.

Farag et al. (2021) found genomic evidence of a novel Asgard Phylum called *Sifarchaeota* in deep marine sediment off the coast of Costa Rica. The study used comparative genomics to show a cluster, *Candidatus* Odinarchaeota within the *Sifarchaeota* Phylum, which contains genes encoding for an incomplete methanogenesis pathway that is coupled to the carbonyl branch of the Wood-Ljunghal pathway. The results suggest that this cluster could be involved with utilizing methylamines. The *Sifarchaeota* metagenome-assembled genomes results found genes for nitrite reductase and sulfate adenylyltransferase and phosphoadenosine phosphosulfate reductase, indicating *Sifarchaeota* could perform nitrite and sulfate reduction. However, their study did not directly link nitrite and sulfate reduction to the utilization of methylamines by *Sifarchaeota*.

Molecular analysis was not performed in the present study; therefore, we are unable to directly link sulfate-reducing or any other heterotrophic bacteria to the direct anaerobic oxidation of methylamine in the SBB. Future work should combine available geochemical and molecular tools to piece together the complexity of metabolisms involved with methylamine turnover and how it may affect the cryptic methane cycle. We note that there appears to be a growing paradigm shift in the understanding of the utilization of non-competitive substrates in anoxic sediment by sulfate-reducing bacteria and methylotrophic methanogens (including other supposedly non-competitive methanogenic substrates like methanol (Sousa et al., 2018; Fischer et al., 2021)). Apparently, methanogens are in fact able to convert these substrates into methane in the presence of their competitors. Which factors provide them this capability should be the subject of future research.

4.4. Implications for cryptic methane cycling in SBB

The SBB is known to have a network of hydrocarbon cold seeps, where methane and other hydrocarbons are released from the lithosphere into the hydro- and atmosphere either perennially or continuously (Hornafius et al., 1999; Leifer et al., 2010; Boles et al., 2004). The migration of methane and other hydrocarbons vertically into the hydrosphere occur along channels that are focused and permeable, such as fault lines and fractures (Moretti, 1998; Smeraglia et al., 2022). Local tectonics and earthquakes could create new fault lines or fractures that reshape or redisperse less permeable sediments, which may open or close migration pathways for hydrocarbons, including methane (Smeraglia et al., 2022). In fact it has been shown that hydrocarbons move much more efficiently through faults when the region in question is seismically active on time scales <100000 yrs (Moretti, 1998). Given the current and historical seismic activity (Probabilities, 1995) and faulting (Boles et al., 2004) within and surrounding the SBB, it is conceivable that hydrocarbon seep patterns and seepage pathways could also shift over time. A potential consequence of this shifting in the SBB is that methane

seepage could spontaneously flow through prior non-seep surface sediment. The fate of this methane would then fall on the methanotrophic communities that are part of the cryptic methane cycle. However, it is not well understood how quickly anaerobic methanotrophs could handle this shift due to their extremely slow growth rates (Knittel and Boetius, 2009; Wilfert et al., 2015; Nauhaus et al., 2007; Dale et al., 2008a). After gaining a better understanding of cryptic methane cycling in the SBB presented in this study, a hypothesis worth testing in future studies is whether cryptic methane cycling based on methylotrophic methanogenesis primes surface sediments to respond faster to increases in methane transport through the sediment.

5. Conclusions

In the present study, we set about to find evidence of cryptic methane cycling in the sulfate-reduction zone of sediment along a depth transect in the oxygen-deficient SBB using a variety of biogeochemical analytics. We found that, within the top 10-20 cm, low methane concentrations were present within sulfate-rich sediment and in the presence of active sulfate reduction. The low methane concentrations were attributed to the balance between methylotrophic methanogenesis and subsequent consumption of the produced methane by AOM. Our results therefore provide strong evidence of cryptic methane cycling in the SBB. We conclude that this important, yet overlooked, process maintains low methane concentrations in surface sediments of this OMZ, and future work should consider cryptic methane cycling in other OMZ's to better constrain carbon cycling in these expanding marine environments.

Our radiotracer analyses further indicated microbial activity that oxidizes monomethylamine directly to CO₂ thereby bypassing methane production. Based off the sulfate reduction activity and methylamine consumption to CO₂ detected in this study and the metagenomic clues presented in the literature, we hypothesize that sulfate reduction may also be supported by methylamines. Our study highlights the metabolic complexity and versatility of anoxic marine sediment near the sediment-water interface within the SBB. Future work should consider how methylamines are consumed by different groups of bacteria and archaea, how methylamine utility by other anaerobic methylotrophs affects the cryptic methane cycle and evaluate if potential environmental changes affect the cryptic methane cycle activity.

Data Availability Statement

- 622 Porewater sulfate concentrations and sulfate reduction rates are accessible through the
- 623 Biological & Chemical Oceanography Data Management Office (BCO-DMO) under the
- 624 following DOI's:
- 625 http://dmoserv3.bco-dmo.org/jg/serv/BCO-DMO/BASIN/porewater_geochemistry.html0,
- 626 http://dmoserv3.bco-dmo.org/jg/serv/BCO-DMO/BASIN/sediment_parameters.html0,
- 627 http://dmoserv3.bco-dmo.org/jg/serv/BCO-DMO/BASIN/microbial_activity.html0.
- Sediment methane concentrations and rates and rate constant data of AOM and methanogenesis
- 629 can be found in the supplementary material Table S2.

630

Author Contributions

- 632 SK and TT designed the study; SK, JL, DY, DR, DH, QQ, FW, and FJ performed experiments
- and made measurements; SK, JL, DY, DR, DH, QQ, FW, FJ, DV, and TT analysed the data;
- 634 SK and TT wrote the manuscript draft with input from all co-authors.

635

636

631

621

Competing Interests

- 637 Some authors are members of the editorial board of Biogeoscience. The peer-review process
- was guided by an independent editor, and the authors have also no other competing interests to
- 639 declare.

640 Acknowledgements

- We thank the captain and crew of R/V Atlantis, the crew of ROV Jason, the crew of AUV
- Sentry, and the science party of the research cruise AT42-19 for their technical and logistical
- support. This work was supported by the National Science Foundation NSF Award NO.: EAR-
- 644 1852912, OCE-1829981 (to TT), and OCE-1830033 (to DV).

References

- Anthony, C.: The biochemistry of methylotrophic micro-organisms, Science Progress (1933-), 167-206, 1975.
- 650 Arndt, S., Lange, C. B., and Berger, W. H.: Climatically controlled marker layers in Santa 651 Barbara Basin sediments and fine-scale core-to-core correlation, Limnology and 652 Oceanography, 35, 165-173, 1990.
- Barnes, R. and Goldberg, E.: Methane production and consumption in anoxic marine sediments, Geology, 4, 297-300, 1976.
- Beulig, F., Røy, H., McGlynn, S. E., and Jørgensen, B. B.: Cryptic CH4 cycling in the sulfate methane transition of marine sediments apparently mediated by ANME-1 archaea,
 The ISME journal, https://doi.org/10.1038/s41396-41018-40273-z, 2018.
- Boetius, A., Ravenschlag, K., Schubert, C. J., Rickert, D., Widdel, F., Giesecke, A., Amann, R.,
 Jørgensen, B. B., Witte, U., and Pfannkuche, O.: A marine microbial consortium
 apparently mediating anaerobic oxidation of methane, Nature, 407, 623-626, 2000.
- Boles, J. R., Eichhubl, P., Garven, G., and Chen, J.: Evolution of a hydrocarbon migration
 pathway along basin-bounding faults: Evidence from fault cement, AAPG bulletin, 88,
 947-970, 2004.
- Cadena, S., García-Maldonado, J. Q., López-Lozano, N. E., and Cervantes, F. J.: Methanogenic
 and sulfate-reducing activities in a hypersaline microbial mat and associated
 microbial diversity, Microbial ecology, 75, 930-940, 2018.
- 667 Canfield, D. E. and Kraft, B.: The 'oxygen'in oxygen minimum zones, Environmental 668 Microbiology, 24, 5332-5344, 2022.
- 669 Capone, D. G., Bronk, D. A., Mulholland, M. R., and Carpenter, E. J.: Nitrogen in the marine 670 environment, Elsevier2008.
- 671 Chistoserdova, L.: Methylotrophs in natural habitats: current insights through 672 metagenomics, Applied microbiology and biotechnology, 99, 5763-5779, 2015.
- 673 Conrad, R.: Contribution of hydrogen to methane production and control of hydrogen 674 concentrations in methanogenic soils and sediments, FEMS microbiology Ecology, 675 28, 193-202, 1999.
- 676 Conrad, R.: Importance of hydrogenotrophic, aceticlastic and methylotrophic 677 methanogenesis for methane production in terrestrial, aquatic and other anoxic 678 environments: a mini review, Pedosphere, 30, 25-39, 2020.
- Dale, A. W., Van Cappellen, P., Aguilera, D., and Regnier, P.: Methane efflux from marine sediments in passive and active margins: Estimations from bioenergetic reaction transport simulations, Earth and Planetary Science Letters, 265, 329-344, 2008a.

- Dale, A. W., Regnier, P., Knab, N. J., Jørgensen, B. B., and Van Cappellen, P.: Anaerobic oxidation of methane (AOM) in marine sediments from the Skagerrak (Denmark): II.
- Reaction-transport modeling, Geochim. Cosmochim. Acta, 72, 2880-2894, 2008b.
- Dale, A. W., Sommer, S., Lomnitz, U., Montes, I., Treude, T., Liebetrau, V., Gier, J., Hensen,
- 686 C., Dengler, M., Stolpovsky, K., Bryant, L. D., and Wallmann, K.: Organic carbon
- 687 production, mineralisation and preservation on the Peruvian margin, Biogeosciences, 688 12, 1537-1559, 2015.
- De Anda, V., Chen, L.-X., Dombrowski, N., Hua, Z.-S., Jiang, H.-C., Banfield, J. F., Li, W.-J., and Baker, B. J.: Brockarchaeota, a novel archaeal phylum with unique and versatile carbon cycling pathways, Nature communications, 12, 1-12, 2021.
- Farag, I. F., Zhao, R., and Biddle, J. F.: "Sifarchaeota," a Novel Asgard Phylum from Costa
 Rican Sediment Capable of Polysaccharide Degradation and Anaerobic
 Methylotrophy, Applied and environmental microbiology, 87, e02584-02520, 2021.
- 695 Ferdelman, T. G., Lee, C., Pantoja, S., Harder, J., Bebout, B. M., and Fossing, H.: Sulfate 696 reduction and methanogenesis in a Thioploca-dominated sediment off the coast of 697 Chile, Geochimica et Cosmochimica Acta, 61, 3065-3079, 1997.
- Fernandes, S., Mandal, S., Sivan, K., Peketi, A., and Mazumdar, A.: Biogeochemistry of Marine Oxygen Minimum Zones with Special Emphasis on the Northern Indian Ocean, Systems Biogeochemistry of Major Marine Biomes, 1-25, 2022.
- Fischer, P. Q., Sánchez-Andrea, I., Stams, A. J., Villanueva, L., and Sousa, D. Z.: Anaerobic microbial methanol conversion in marine sediments, Environmental microbiology, 23, 1348-1362, 2021.
- Gibb, S. W., Mantoura, R. F. C., Liss, P. S., and Barlow, R. G.: Distributions and
 biogeochemistries of methylamines and ammonium in the Arabian Sea, Deep Sea
 Research Part II: Topical Studies in Oceanography, 46, 593-615, 1999.
- Hanson, R. S. and Hanson, T. E.: Methanotrophic bacteria, Microbiol. Rev., 60, 439-471, 1996.
- Helly, J. J. and Levin, L. A.: Global distribution of naturally occurring marine hypoxia on continental margins, Deep Sea Research Part I: Oceanographic Research Papers, 51, 1159-1168, 2004.
- Hinrichs, K.-U. and Boetius, A.: The anaerobic oxidation of methane: new insights in
- microbial ecology and biogeochemistry, in: Ocean Margin Systems, edited by: Wefer,
- G., Billett, D., Hebbeln, D., Jørgensen, B. B., Schlüter, M., and Van Weering, T.,
- 715 Springer-Verlag, Berlin, 457-477, 2002.

- Hoehler, T. M., Alperin, M. J., Albert, D. B., and Martens, C. S.: Apparent minimum free energy requirements for methanogenic Archaea and sulfate-reducing bacteria in an anoxic marine sediment, FEMS Microbiol. Ecol., 38, 33-41, 2001.
- Hornafius, J. S., Quigley, D., and Luyendyk, B. P.: The world's most spectacular marine hydrocarbon seeps (Coal Oil Point, Santa Barbara Channel, California): Quantification of emissions, Journal of Geophysical Research: Oceans, 104, 20703-20711, 1999.
- Joye, S. B., Boetius, A., Orcutt, B. N., Montoya, J. P., Schulz, H. N., Erickson, M. J., and Logo, S. K.: The anaerobic oxidation of methane and sulfate reduction in sediments from Gulf of Mexico cold seeps, Chem. Geol., 205, 219-238, 2004.
- Jørgensen, B. B.: A comparison of methods for the quantification of bacterial sulphate reduction in coastal marine sediments: I. Measurements with radiotracer techniques, Geomicrobiol. J., 1, 11-27, 1978.
- Jørgensen, B. B.: Bacteria and marine biogeochemistry, in: Marine biogeochemistry, edited by: Schulz, H. D., and Zabel, M., Springer Verlag, Berlin, 173-201, 2000.
- 730 Kallmeyer, J., Ferdelman, T. G., Weber, A., Fossing, H., and Jørgensen, B. B.: A cold 731 chromium distillation procedure for radiolabeled sulfide applied to sulfate reduction 732 measurements, Limnol. Oceanogr. Methods, 2, 171-180, 2004.
- King, G., Klug, M. J., and Lovley, D. R.: Metabolism of acetate, methanol, and methylated amines in intertidal sediments of Lowes Cove, Maine, 45, 1848-1853, 1983.
- Kivenson, V., Paul, B. G., and Valentine, D. L.: An ecological basis for dual genetic code expansion in marine deltaproteobacteria, Frontiers in microbiology, 1545, 2021.
- Knittel, K. and Boetius, A.: Anaerobic oxidation of methane: progress with an unknown process, Annu. Rev. Microbiol., 63, 311-334, 2009.
- Kononets, M., Tengberg, A., Nilsson, M., Ekeroth, N., Hylén, A., Robertson, E. K., Van De Velde, S., Bonaglia, S., Rütting, T., and Blomqvist, S.: In situ incubations with the Gothenburg benthic chamber landers: Applications and quality control, Journal of Marine Systems, 214, 103475, 2021.
- Krause, S. J. and Treude, T.: Deciphering cryptic methane cycling: Coupling of
 methylotrophic methanogenesis and anaerobic oxidation of methane in hypersaline
 coastal wetland sediment, Geochimica et Cosmochimica Acta, 302, 160-174, 2021.
- Kristjansson, J. K., Schönheit, P., and Thauer, R. K.: Different Ks values for hydrogen of methanogenic bacteria and sulfate reducing bacteria: an explanation for the apparent inhibition of methanogenesis by sulfate, Arch. Microbiol., 131, 278-282, 1982.
- Lee, C. and Olson, B. L.: Dissolved, exchangeable and bound aliphatic amines in marine sediments: initial results, Organic Geochemistry, 6, 259-263, 1984.

- Leifer, I., Kamerling, M. J., Luyendyk, B. P., and Wilson, D. S.: Geologic control of natural
 marine hydrocarbon seep emissions, Coal Oil Point seep field, California, Geo-Marine
 Letters, 30, 331-338, 2010.
- Levin, L.: Oxygen minimum zone benthos: Adaptation and community response to hypoxia, Oceanogr. Mar. Biol. Ann. Rev., 41, 1-45, 2003.
- Levin, L. A. E., W., Gooday, A. J., Jorissen, F., Middelburg, J. J., Naqvi, S. W. A., Neira, C., and Rabalais, N. N. Z., J.: Effects of natural and human-induced hypoxia on coastal benthos, Biogeosciences, 6, 2063–2098, 2009.
- Lovley, D. R. and Klug, M. J.: Model for the distribution of sulfate reduction and methanogenesis in freshwater sediments, Geochim. Cosmochim. Acta, 50, 11-18, 1986.
- Lyu, Z., Shao, N., Akinyemi, T., and Whitman, W. B.: Methanogenesis, Current Biology, 28, R727-R732, 2018.
- Maltby, J., Sommer, S., Dale, A. W., and Treude, T.: Microbial methanogenesis in the sulfatereducing zone of surface sediments traversing the Peruvian margin, Biogeosciences, 13, 283–299, 2016.
- Maltby, J., Steinle, L., Löscher, C. R., Bange, H. W., Fischer, M. A., Schmidt, M., and Treude,
 T.: Microbial methanogenesis in the sulfate-reducing zone of sediments in the
 Eckernförde Bay, SW Baltic Sea, Biogeosciences, 15, 137–157, 2018.
- Mausz, M. A. and Chen, Y.: Microbiology and ecology of methylated amine metabolism in marine ecosystems, Current Issues in Molecular Biology, 33, 133-148, 2019.
- Michaelis, W., Seifert, R., Nauhaus, K., Treude, T., Thiel, V., Blumenberg, M., Knittel, K.,
 Gieseke, A., Peterknecht, K., Pape, T., Boetius, A., Aman, A., Jørgensen, B. B., Widdel,
 F., Peckmann, J., Pimenov, N. V., and Gulin, M.: Microbial reefs in the Black Sea
 fueled by anaerobic oxidation of methane, Science, 297, 1013-1015, 2002.
- Middelburg, J. J. and Levin, L. A.: Coastal hypoxia and sediment biogeochemistry, Biogeosciences, 6, 1273-1293, 2009.
- Moretti, I.: The role of faults in hydrocarbon migration, Petroleum Geoscience, 4, 81-94, 1998.
- Nauhaus, K., Albrecht, M., Elvert, M., Boetius, A., and Widdel, F.: In vitro cell growth of marine archaeal-bacterial consortia during anaerobic oxidation of methane with sulfate, Environ. Microbiol., 9, 187-196, 2007.
- Oremland, R. S. and Polcin, S.: Methanogenesis and sulfate reduction: competitive and noncompetitive substrates in estuarine sediments, Appl. Environ. Microbiol., 44, 1270-1276, 1982.

- Oremland, R. S. and Taylor, B. F.: Sulfate reduction and methanogenesis in marine sediments, Geochimica et Cosmochimica Acta, 42, 209-214, 1978.
- Oremland, R. S., Marsh, L. M., and Polcin, S.: Methane production and simultaneous sulphate reduction in anoxic, salt marsh sediments, Nature, 296, 143-145, 1982.
- Oren, A.: Formation and breakdown of glycine betaine and trimethylamine in hypersaline environments, Antonie van Leeuwenhoek, 58, 291-298, 1990.
- Orphan, V. J., Hinrichs, K.-U., Ussler III, W., Paull, C. K., Tayleor, L. T., Sylva, S. P., Hayes, J. M., and DeLong, E. F.: Comparative analysis of methane-oxidizing archaea and sulfatereducing bacteria in anoxic marine sediments, Appl. Environ. Microbiol., 67, 1922-1934, 2001.
- Paulmier, A. and Ruiz-Pino, D.: Oxygen minimum zones (OMZs) in modern ocean, Progr. Oceanog., 80, 113-128, 2009.
- Probabilities, W. G. o. C. E.: Seismic hazards in southern California: probable earthquakes, 1994 to 2024, Bulletin of the Seismological Society of America, 85, 379-439, 1995.
- Qin, Q., Kinnaman, F. S., Gosselin, K. M., Liu, N., Treude, T., and Valentine, D. L.: Seasonality of water column methane oxidation and deoxygenation in a dynamic marine environment, Geochimica et Cosmochimica Acta, 336, 219-230, 2022.
- Ragsdale, S. W. and Pierce, E.: Acetogenesis and the Wood–Ljungdahl pathway of CO2 fixation, Biochimica et Biophysica Acta (BBA)-Proteins and Proteomics, 1784, 1873-1898, 2008.
- Reeburgh, W. S.: Oceanic methane biogeochemistry, Chem. Rev., 107, 486-513, 2007.
- Reimers, C. E., Ruttenberg, K. C., Canfield, D. E., Christiansen, M. B., and Martin, J. B.:

 Porewater pH and authigenic phases formed in the uppermost sediments of Santa
 Barbara Basin, Geochim. Cosmochim. Acta, 60, 4037-4057, 1996.
- Rullkötter, J.: Organic matter: the driving force for early diagenesis, in: Marine geochemistry, Springer, 125-168, 2006.
- Schimmelmann, A. and Kastner, M.: Evolutionary changes over the last 1000 years of reduced sulfur phases and organic carbon in varved sediments of the Santa Barbara Basin, California, Geochimica et Cosmochimica Acta, 57, 67-78, 1993.
- Sholkovitz, E.: Interstitial water chemistry of the Santa Barbara Basin sediments, Geochimica et Cosmochimica Acta, 37, 2043-2073, 1973.
- Smeraglia, L., Fabbi, S., Billi, A., Carminati, E., and Cavinato, G. P.: How hydrocarbons move along faults: Evidence from microstructural observations of hydrocarbon-bearing carbonate fault rocks, Earth and Planetary Science Letters, 584, 117454, 2022.
- Sousa, D. Z., Visser, M., Van Gelder, A. H., Boeren, S., Pieterse, M. M., Pinkse, M. W., Verhaert, P. D., Vogt, C., Franke, S., and Kümmel, S.: The deep-subsurface sulfate

- reducer Desulfotomaculum kuznetsovii employs two methanol-degrading pathways,
 Nature communications, 9, 1-9, 2018.
- Soutar, A. and Crill, P. A.: Sedimentation and climatic patterns in the Santa Barbara Basin during the 19th and 20th centuries, Geological Society of America Bulletin, 88, 1161-1172, 1977.
- Stephenson, M. and Stickland, L. H.: CCVII. Hydrogenase. III. The bacterial formation of methane by the reduction of one-carbon compounds by molecular hydrogen, Biochem. J., 27, 1517–1527, 1933.
- Taubert, M., Grob, C., Howat, A. M., Burns, O. J., Pratscher, J., Jehmlich, N., von Bergen, M., Richnow, H. H., Chen, Y., and Murrell, J. C.: Methylamine as a nitrogen source for microorganisms from a coastal marine environment, Environmental microbiology, 19, 2246-2257, 2017.
- Thauer, R. K.: Biochemistry of methanogenesis: a tribute to Marjory Stephenson, Microbiology, 144, 2377-2406, 1998.
- Treude, T.: Biogeochemical reactions in marine sediments underlying anoxic water bodies, in: Anoxia: Paleontological Strategies and Evidence for Eukaryote Survival, edited by: Altenbach, A., Bernhard, J., and Seckbach, J., Cellular Origins, Life in Extreme Habitats and Astrobiology (COLE) Book Series, Springer, Dordrecht, 18-38, 2011.
- Treude, T., Krüger, M., Boetius, A., and Jørgensen, B. B.: Environmental control on anaerobic oxidation of methane in the gassy sediments of Eckernförde Bay (German Baltic),
 Limnol. Oceanogr., 50, 1771-1786, 2005.
- Treude, T., Smith, C. R., Wenzhoefer, F., Carney, E., Bernardino, A. F., Hannides, A. K., Krueger, M., and Boetius, A.: Biogeochemistry of a deep-sea whale fall: sulfate reduction, sulfide efflux and methanogenesis, Mar. Ecol. Prog. Ser., 382, 1-21, 2009.
- Wang, X.-c. and Lee, C.: The distribution and adsorption behavior of aliphatic amines in marine and lacustrine sediments, Geochimica et Cosmochimica Acta, 54, 2759-2774, 1990.
- Wang, X.-C. and Lee, C.: Adsorption and desorption of aliphatic amines, amino acids and acetate by clay minerals and marine sediments, Marine Chemistry, 44, 1-23, 1993.
- Wang, X.-C. and Lee, C.: Sources and distribution of aliphatic amines in salt marsh sediment,
 Organic Geochemistry, 22, 1005-1021, 1994.
- Wehrmann, L. M., Risgaard-Petersen, N., Schrum, H. N., Walsh, E. A., Huh, Y., Ikehara, M.,
- Pierre, C., D'Hondt, S., Ferdelman, T. G., and Ravelo, A. C.: Coupled organic and
- inorganic carbon cycling in the deep subseafloor sediment of the northeastern
- 857 Bering Sea Slope (IODP Exp. 323), Chemical Geology, 284, 251-261, 2011.

- Wilfert, P., Krause, S., Liebetrau, V., Schönfeld, J., Haeckel, M., Linke, P., and Treude, T.:
 Response of anaerobic methanotrophs and benthic foraminifera to 20 years of
 methane emission from a gas blowout in the North Sea, Marine and Petroleum
 Geology, 68, 731-742, 2015.
- Winfrey, M. R. and Ward, D. M.: Substrates for sulfate reduction and methane p roduction in intertidal sediments, Appl. Environm. Microbiol, 45, 193-199, 1983.
- Wright, J. J., Konwar, K. M., and Hallam, S. J.: Microbial ecology of expanding oxygen minimum zones, Nature Reviews Microbiology, 10, 381-394, 2012.
- Wyrtki, K.: The oxygen minima in relation to ocean circulation, Deep Sea Research and Oceanographic Abstracts, 11-23,
- Xiao, K., Beulig, F., Kjeldsen, K., Jorgensen, B., and Risgaard-Petersen, N.: Concurrent
 Methane Production and Oxidation in Surface Sediment from Aarhus Bay, Denmark,
 Frontiers in Microbiology, 8, 10.3389/fmicb.2017.01198, 2017.
- Xiao, K., Beulig, F., Roy, H., Jorgensen, B., and Risgaard-Petersen, N.: Methylotrophic methanogenesis fuels cryptic methane cycling in marine surface sediment, Limnology and Oceanography, 63, 1519-1527, 10.1002/lno.10788, 2018.
- Xiao, K.-Q., Moore, O. W., Babakhani, P., Curti, L., and Peacock, C. L.: Mineralogical control
 on methylotrophic methanogenesis and implications for cryptic methane cycling in
 marine surface sediment, Nature Communications, 13, 1-9, 2022.
- Zhuang, G.-C., Montgomery, A., and Joye, S. B.: Heterotrophic metabolism of C1 and C2 low
 molecular weight compounds in northern Gulf of Mexico sediments: Controlling
 factors and implications for organic carbon degradation, Geochimica et
 Cosmochimica Acta, 247, 243-260, 2019.
- Zhuang, G.-C., Elling, F. J., Nigro, L. M., Samarkin, V., Joye, S. B., Teske, A., and Hinrichs, K.U.: Multiple evidence for methylotrophic methanogenesis as the dominant
 methanogenic pathway in hypersaline sediments from the Orca Basin, Gulf of
 Mexico, Geochim. Cosmochim. Acta, 187, 1-20, 2016.
- Zhuang, G.-C., Lin, Y.-S., Bowles, M. W., Heuer, V. B., Lever, M. A., Elvert, M., and Hinrichs,
 K.-U.: Distribution and isotopic composition of trimethylamine, dimethylsulfide and
 dimethylsulfoniopropionate in marine sediments, Mar. Chem., 196, 35-46, 2017.
- Zhuang, G.-C., Heuer, V. B., Lazar, C. S., Goldhammer, T., Wendt, J., Samarkin, V. A., Elvert,
 M., Teske, A. P., Joye, S. B., and Hinrichs, K.-U.: Relative importance of
 methylotrophic methanogenesis in sediments of the Western Mediterranean Sea,
 Geochim. Cosmochim. Acta, 224, 2018.

Supplemental Material

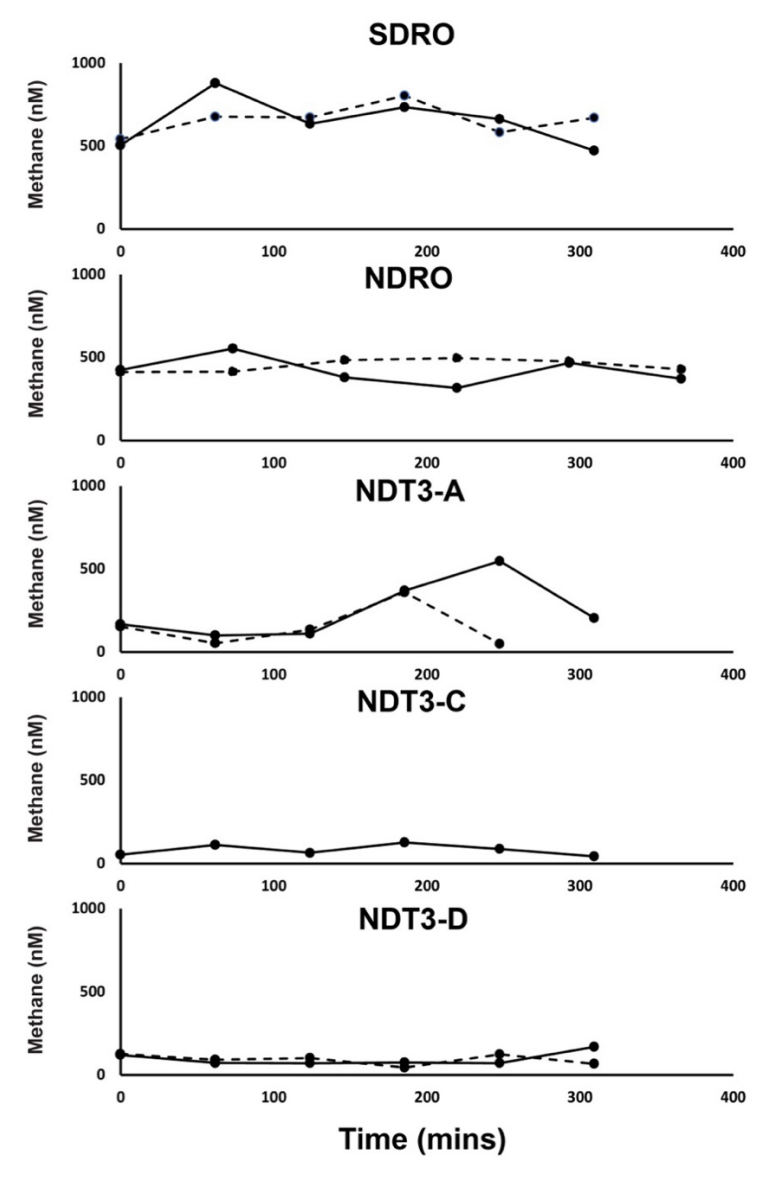


Figure S1. Methane concentrations from benthic flux chamber experiments across the depth transect of the Santa Barbara Basin. Solid lines are methane concentrations from benthic flux chamber 1. Dashed lines are methane concentrations from benthic flux chamber 2.

Table S1. Porewater concentrations of acetate, methanol and methylamine detected within two sediment intervals at each station sampled in this study.

Station, Sediment Depth (cm)	Acetate (µM)	Methanol (μM)	Methylamine (μM)
SDRO, 1-2cm	BQ	BD	BQ
SDRO, 9-10 cm	BD	BD	BD
NDRO, 1-2 cm	BQ	BD	BD
NDRO, 9-10 cm	BD	BD	BD
NDT3-A, 1-2 cm	21	BQ	BQ
NDT3-A, 9-10 cm	BD	BD	BD
NDT3-C, 1-2 cm	BD	BD	BD
NDT3-C, 9-10 cm	BD	BD	BD
NDT3-D, 1-2 cm	BD	BD	BD
NDT3-D, 9-10 cm	BD	BD	BD

Table S2. Porewater concentrations of methane and ex situ rate data and rate constants (k) of AOM from directly from ¹⁴C-CH₄ (AOM- CH₄), AOM derived from ¹⁴C-mono-methylamine (AOM-MMA), and methanogenesis from ¹⁴C-mono-methylamine (MG-MMA).

SDRO	Station	Sediment Depth For methane (cm)	Methane (μM)	Sediment Depth for Rates (cm)	AOM-CH4 (nmol cm ⁻³ d ⁻¹)	AOM-CH4 k (d-1)	AOM-MMA (nmol cm ⁻³ d ⁻¹)	AOM-MMA k (d-1)	MG-MMA (nmol cm ⁻³ d ⁻¹)	MG-MMA k (d ⁻¹)
SDR0										0.13
SORIO 2.5 5.56 2.5 0.03 0.00 6.03 0.92 0.29										0.15
SORIO 4.5 7.65 4.5 0.00 0.00 7.02 0.92 0.32 SORIO 5.5 5.88 5.5 0.01 0.00 5.37 0.92 0.41 SORIO 6.5 10.89 6.5 0.00 0.00 0.00 10.02 0.92 0.31 SORIO 7.5 10.12 7.5 0.00 0.00 0.00 10.02 0.92 0.31 SORIO 7.5 10.12 7.5 0.00 0.00 0.00 0.00 0.00 0.00 0.03 38 SORIO 8.5 - 8.5 0.01 0.00 0.00 0.00 0.00 0.00 0.00 0.										0.10
SDRO	SDRO		5.68	3.5	0.01				0.18	0.06
SPRICE 1.05 10.89 6.5 0.00 0.00 10.02 0.92 0.31										0.11
SORRO 8.5 - 8.5 0.01 0.00 0.00 9.31 0.92 0.29 SORRO 9.5 - 9.5 0.01 0.00 0.00 0.00 0.03 SORRO 11 - 10.5 0.02 0.00 9.14 0.90 0.02 SORRO 13 - 11.5 0.00 0.00 0.00 9.15 0.90 SORRO 13 - 11.5 0.00 0.00 0.00 9.17 0.90 SORRO 13 - 11.5 0.00 0.00 0.00 9.17 0.90 SORRO 17 - 12.5 0.00 0.00 0.00 9.17 0.90 SORRO 17 - 12.5 0.00 0.00 0.00 0.00 0.00 SORRO 17 - 12.5 0.00 0.00 0.00 0.00 0.00 SORRO 17 - 12.5 0.00 0.00 0.00 0.00 0.00 SORRO 19 - 14.5 0.00 0.00 0.00 0.00 0.00 SORRO 19 - 14.5 0.00 0.00 0.00 0.00 0.00 0.00 SORRO 15 - 11.00 1.5 0.05 0.00 0.00 0.00 0.00 0.00										0.14
SORIO S. - S. 0.01										0.10
SDRO 9.5 - 9.5 0.01 0.00 0.00 0.00 0.28			10.12							0.10
SDRO			-							0.11 0.09
SDRO			-							
SDRO								0.00		0.09 0.10
SDRO 17 - 14.5 0.00 0.00 9.17 0.91 0.27 SDRO 19 - 14.5 0.00 0.00 0.00 0.00 0.00 0.26 NDRO 0.5 5.96 0.5 0.05 0.05 0.01 5.31 0.89 0.41 NDRO 1.5 11.10 1.5 0.05 0.00 0.00 0.00 0.00										0.08
SPRICE 19										0.09
NDRO 0.5 5.96 0.5 0.05 0.01 5.31 0.89 0.41 NDRO 1.5 11.10 1.5 0.05 0.00 0.00 0.00 0.00	SDRO			14.5	0.00	0.00	0.00	0.00	0.26	0.09
NDRO			5.96							0.14
NDRO	NDRO	1.5	11.10		0.05	0.00	0.00	0.00	0.29	0.10
NDRO	NDRO	2.5	3.55	2.5	0.00	0.00	0.00	0.00	0.28	0.09
NDRO 5.5 9.26 5.5 0.00 0.00 8.35 0.90 0.34 NDRO 6.5 8.28 6.5 0.00 0.00 0.00 0.00 0.03 NDRO 7.5 7.67 7.5 0.00 0.00 0.00 0.00 0.03 NDRO 8.5 9.51 8.5 0.00 0.00 0.00 0.00 0.03 NDRO 9.5 5.33 9.5 0.00 0.00 0.00 0.00 0.02 NDRO 11 10.46 10.5 0.00 0.00 0.00 0.00 0.02 NDRO 13 5.58 11.5 0.01 0.00 0.00 0.00 0.00 0.02 NDRO 15 7.51 12.5 0.00 0.00 0.00 0.00 0.02 NDRO 17 13.56 13.5 0.00 0.00 0.00 0.00 0.02 NDRO 19 15.68 14.5 0.00 0.00 0.00 0.00 0.00 0.21 NDRO 19 15.68 14.5 0.00 0.00 0.00 0.00 0.00 0.01 NDT3-A 0.5 7.88 0.5 0.03 0.00 7.09 0.90 0.45 NDT3-A 1.5 5.66 1.5 0.07 0.01 5.09 0.90 0.41 NDT3-A 3.5 4.03 3.5 0.00 0.00 0.00 3.62 0.90 0.27 NDT3-A 4.5 7.92 4.5 0.01 0.00 0.00 7.11 0.90 0.33 NDT3-A 5.5 2.68 5.5 0.00 0.00 0.00 7.11 0.90 0.33 NDT3-A 6.5 8.81 6.5 0.00 0.00 0.00 7.78 0.90 0.34 NDT3-A 6.5 8.81 6.5 0.00 0.00 7.78 0.90 0.32 NDT3-A 8.5 8.70 8.5 0.00 0.00 7.78 0.90 0.32 NDT3-A 11 5.29 10.5 0.00 0.00 0.00 0.00 0.02 NDT3-A 15 5.21 2.5 0.00 0.00 0.00 0.00 0.02 NDT3-A 15 5.29 1.50 0.00 0.00 0.00 0.00 0.02 NDT3-A 15 5.29 1.50 0.00 0.00 0.00 0.00 0.02 NDT3-A 15 5.75 0.00 0.00 0.00 0.00 0.00 0.02 NDT3-A 15 5.75 0.00 0.00 0.00 0.00 0.00 0.00 0.00 NDT3-A 15 5.21 5.5 5.21 0.5 6.8 0.00 0.00 0.00 0.00 0.00 0.00 0.00 NDT3-A 15 5.29 10.5 0.00 0.00 0.00 0.00 0.00 0.00 0.00 0.00 NDT3-A 15 5.21 5.5 5.21 5.5 5.21 5.5 5.21 5.5 5.21 5.5 5.21 5.5 5.21 5.5 5.21 5.5 5.21 5.5 5.21 5.5 5.21 5.5 5.21 5.5 5.21 5.5 5.21 5.5 5.21 5.5 5.21 5.5 5.21 5.5 5.21 5.5 5.21	NDRO		11.72		0.02	0.00	0.00	0.00	0.31	0.10
NDRO 6.5										0.14
NDRO 7.5										0.11
NDRO 8.5										0.12
NDRO										0.12
NDRO										0.10
NDRO										0.07
NDRO 15 7.51 12.5 0.00 0.00 0.00 0.00 0.00 0.25 NDRO 17 13.56 13.5 0.00 0.00 0.00 0.00 0.00 0.25 NDRO 19 15.68 14.5 0.00 0.00 0.00 7.09 0.90 0.45 NDRO 11 15.68 15.5 0.07 0.01 5.09 0.90 0.45 NDRO 13 15.566 15.5 0.07 0.01 5.09 0.90 0.45 NDRO 13 2.5 5.21 2.5 0.04 0.01 4.66 0.90 0.27 NDRO 13 3.5 4.03 3.5 0.00 0.00 3.62 0.90 0.27 NDRO 13 4 5.5 7.92 4.5 0.01 0.00 7.11 0.90 0.33 NDRO 13 4 5.5 7.92 4.5 0.01 0.00 7.11 0.90 0.33 NDRO 13 4 5.5 2.68 5.5 0.00 0.00 2.40 0.90 0.34 NDRO 13 4 5.5 2.88 5.5 0.00 0.00 2.40 0.90 0.34 NDRO 13 4 5.5 2.88 5.5 0.00 0.00 7.91 0.90 0.32 NDRO 13 4 5.5 2.88 5.5 0.00 0.00 7.91 0.90 0.32 NDRO 13 4 5.5 2.89 0.55 0.00 0.00 7.91 0.90 0.32 NDRO 13 4 5.5 2.89 0.55 0.00 0.00 7.78 0.89 0.24 NDRO 13 4 5.5 2.5 0.00 0.00 0.00 7.78 0.89 0.24 NDRO 13 4 15 5.29 10.5 0.00 0.00 0.00 7.78 0.89 0.24 NDRO 13 4 11 5.29 10.5 0.00 0.00 0.00 1.00 0.00 0.00 NDRO 13 4 13 - 11.5 0.00 0.00 0.00 0.00 0.00 0.00 NDRO 13 4 15 - 12.5 0.00 0.00 0.00 0.00 0.00 0.00 NDRO 13 4 17 - 13.5 0.00 0.00 0.00 0.00 0.00 0.00 NDRO 13 4 17 - 13.5 0.00 0.00 0.00 0.00 0.00 0.00 NDRO 15 8.47 1.5 0.88 0.1 6.94 0.82 0.25 NDRO 15 8.47 1.5 0.88 0.1 6.94 0.82 0.22 NDRO 15 8.47 1.5 0.88 0.1 6.94 0.82 0.22 NDRO 15 8.47 1.5 0.88 0.1 6.94 0.82 0.22 NDRO 15 8.47 1.5 0.98 0.01 0.00 0.00 0.00 0.00 0.00 0.00 NDRO 15 8.5 5.5 5.99 4.5 0.05 0.01 4.88 0.81 0.22 NDRO 16 9.5 5.5 6.79 5.5 0.07 0.01 0.00 0.00 0.00 0.00 0.00 NDRO 16 9.5 5.5 0.72 6.5 0.02 0.00 5.66 0.79 0.82 0.28 NDRO 16 0.5 5.5 0.72 6.5 0.02 0.00 5.66 0.79 0.92 0.22 NDRO 16 0.5 0.5 0.5 0.1 4.88 0.81 0.22 NDRO 17 0.5 0.5 0.5 0.1 4.88 0.81 0.22 NDRO 18 0.5 0.5 0.1 4.88 0.81 0.25 NDRO 18 0.5 0.5 0.00 0.00 0.00 0.00 0.00 0.00										0.07
NDRO						0.00	0.00	0.00		0.08
NDRO										0.07
NDT3-A							0.00	0.00	0.21	0.07
NDT3-A							7.09	0.90	0.45	0.15
NDT3-A 3.5										0.14
NDT3-A	NDT3-A	2.5	5.21	2.5	0.04	0.01	4.66	0.90	0.27	0.09
NDT3-A 5.5 2.68 5.5 0.00 0.00 2.40 0.90 0.34 NDT3-A 6.5 8.81 6.5 0.00 0.00 7.91 0.90 0.32 NDT3-A 6.5 8.81 6.5 0.00 0.00 7.91 0.90 0.32 NDT3-A 7.5 4.05 7.5 0.00 0.00 3.64 0.90 0.32 NDT3-A 8.5 8.70 8.5 0.00 0.00 7.78 0.89 0.24 NDT3-A 8.5 8.70 8.5 0.00 0.00 0.00 7.78 0.89 0.24 NDT3-A 11 5.29 10.5 0.00 0.00 0.00 4.14 0.90 0.24 NDT3-A 11 5.29 10.5 0.00 0.00 0.00 0.00 0.00 0.00 0.00	NDT3-A	3.5	4.03	3.5	0.00	0.00	3.62	0.90	0.29	0.10
NDT3-A 6.5 8.81 6.5 0.00 0.00 7.91 0.90 0.32 NDT3-A 7.5 4.05 7.5 0.00 0.00 3.64 0.90 0.32 NDT3-A 8.5 8.70 8.5 0.00 0.00 7.78 0.89 0.24 NDT3-A 9.5 4.62 9.5 0.00 0.00 0.00 4.14 0.90 0.24 NDT3-A 11 5.29 10.5 0.00 0.00 0.00 4.14 0.90 0.24 NDT3-A 11 5.29 10.5 0.00 0.00 0.00 0.00 0.00 0.00 0.18 NDT3-A 13 - 11.5 0.00 0.00 4.71 0.89 0.27 NDT3-A 15 - 12.5 0.00 0.00 0.00 0.00 0.00 0.00 0.25 NDT3-A 17 - 13.5 0.00 0.00 0.00 0.00 0.00 0.00 0.00 NDT3-A 19 - 14.5 0.00 0.00 0.00 0.00 0.00 0.00 0.00 NDT3-A 19 - 14.5 0.00 0.00 0.00 0.00 0.00 0.00 0.00 NDT3-C 0.5 5.21 0.5 1.68 0.32 4.28 0.82 0.33 NDT3-C 1.5 8.47 1.5 0.08 0.01 6.94 0.82 0.26 NDT3-C 2.5 9.38 2.5 0.06 0.01 6.94 0.82 0.26 NDT3-C 3.5 5.82 3.5 0.33 0.06 4.79 0.82 0.28 NDT3-C 4.5 5.99 4.5 0.05 0.01 4.88 0.81 0.22 NDT3-C 5.5 6.79 5.5 0.07 0.01 0.00 0.00 0.00 0.00 NDT3-C 8.5 11.10 8.5 0.05 0.01 4.88 0.81 0.22 NDT3-C 7.5 7.25 7.5 0.03 0.00 0.00 0.00 0.00 0.00 NDT3-C 8.5 11.10 8.5 0.13 0.01 9.77 0.83 0.19 NDT3-C 8.5 11.10 8.5 0.13 0.01 9.77 0.83 0.19 NDT3-C 15 7.73 12.5 0.01 0.00 5.69 0.79 0.22 NDT3-C 15 7.73 12.5 0.00 0.00 5.69 0.79 0.22 NDT3-C 15 7.73 12.5 0.00 0.00 0.00 0.00 0.00 0.00 0.00 0	NDT3-A	4.5	7.92	4.5	0.01	0.00	7.11	0.90	0.33	0.11
NDT3-A 7.5 4.05 7.5 0.00 0.00 3.64 0.90 0.32 NDT3-A 8.5 8.70 8.5 0.00 0.00 7.78 0.89 0.24 NDT3-A 8.5 8.70 8.5 0.00 0.00 4.14 0.90 0.24 NDT3-A 11 5.29 10.5 0.00 0.00 4.14 0.90 0.24 NDT3-A 11 5.29 10.5 0.00 0.00 0.00 0.00 0.00 0.00 0.18 NDT3-A 11 5.29 10.5 0.00 0.00 0.00 0.00 0.00 0.00 0.00							21.10	0.00		0.11
NDT3-A 8.5 8.70 8.5 0.00 0.00 7.78 0.89 0.24 NDT3-A 9.5 4.62 9.5 0.00 0.00 0.00 4.14 0.90 0.24 NDT3-A 11 5.29 10.5 0.00 0.00 0.00 0.00 0.00 0.00 NDT3-A 13 - 11.5 0.00 0.00 0.00 0.00 0.00 0.00 NDT3-A 15 - 12.5 0.00 0.00 0.00 0.00 0.00 0.00 NDT3-A 17 - 13.5 0.00 0.00 0.00 0.00 0.00 0.00 NDT3-A 19 - 14.5 0.00 0.00 0.00 0.00 0.00 0.00 NDT3-A 19 - 14.5 0.00 0.00 0.00 0.00 0.00 0.00 0.00 NDT3-C 0.5 5.21 0.5 1.68 0.32 4.28 0.82 0.33 NDT3-C 1.5 8.47 1.5 0.08 0.01 6.94 0.82 0.26 NDT3-C 2.5 9.38 2.5 0.06 0.01 0.00 0.00 0.00 0.00 NDT3-C 3.5 5.82 3.5 0.33 0.06 4.79 0.82 0.28 NDT3-C 4.5 5.99 4.5 0.05 0.01 4.88 0.81 0.22 NDT3-C 6.5 7.22 6.5 0.00 0.00 0.00 0.00 0.00 0.00 NDT3-C 8.5 11.10 8.5 0.07 0.01 0.00 0.00 0.00 NDT3-C 8.5 11.10 8.5 0.13 0.01 9.17 0.83 0.19 NDT3-C 7.5 7.25 7.5 0.03 0.00 0.00 0.00 0.00 0.01 NDT3-C 8.5 11.10 8.5 0.13 0.01 9.17 0.83 0.19 NDT3-C 11 7.24 9.5 0.01 0.00 5.69 0.79 0.22 NDT3-C 15 7.73 12.5	NDT3-A	6.5	8.81	6.5	0.00	0.00	7.91	0.90	0.32	0.11
NDT3-A 9.5 4.62 9.5 0.00 0.00 4.14 0.90 0.24 NDT3-A 11 5.29 10.5 0.00 0.00 0.00 0.00 0.00 0.18 NDT3-A 13 - 11.5 0.00 0.00 0.00 4.71 0.89 0.27 NDT3-A 15 - 12.5 0.00 0.00 0.00 0.00 0.00 0.00 0.25 NDT3-A 17 - 13.5 0.00 0.00 0.00 0.00 0.00 0.00 0.00 0	NDT3-A	7.5	4.05	7.5	0.00	0.00	3.64	0.90	0.32	0.11
NDT3-A 11 5.29 10.5 0.00 0.00 0.00 0.00 0.00 0.18 NDT3-A 13 - 11.5 0.00 0.00 0.00 0.00 0.00 0.00 0.00	NDT3-A						7.78			0.08
NDT3-A 13								0.00		0.08
NDT3-A 15 - 12.5 0.00 0.00 0.00 0.00 0.00 0.05 NDT3-A 17 - 13.5 0.00 0.00 0.00 0.00 0.00 0.00 0.00 NDT3-A 19 - 14.5 0.00 0.00 0.00 0.00 0.00 0.00 0.00 0			5.29							0.06
NDT3-A 17 - 13.5 0.00 0.00 0.00 0.00 0.00 0.00 NDT3-A 19 - 14.5 0.00 0.00 0.00 0.00 0.00 0.26 NDT3-A 19 - 14.5 0.00 0.00 0.00 0.00 0.00 0.26 NDT3-C 0.5 5.21 0.5 1.68 0.32 4.28 0.82 0.33 NDT3-C 1.5 8.47 1.5 0.08 0.01 6.94 0.82 0.26 NDT3-C 2.5 9.38 2.5 0.06 0.01 0.00 0.00 0.00 0.00 0.00 NDT3-C 3.5 5.82 3.5 0.33 0.06 4.79 0.82 0.28 NDT3-C 4.5 5.99 4.5 0.05 0.01 0.00 0.00 0.00 0.00 0.05 NDT3-C 5.5 6.79 5.5 0.07 0.01 0.00 0.00 0.00 0.05 NDT3-C 6.5 7.22 6.5 0.02 0.00 5.66 0.78 0.19 NDT3-C 7.5 7.25 7.5 0.03 0.00 0.00 0.00 0.00 0.05 NDT3-C 8.5 11.10 8.5 0.13 0.01 9.17 0.83 0.19 NDT3-C 9.5 7.24 9.5 0.01 0.00 5.69 0.79 0.22 NDT3-C 11 7.24 10.5 0.04 0.01 5.14 0.71 0.22 NDT3-C 13 6.38 11.5 NDT3-C 15 7.73 12.5 NDT3-C 15 7.73 12.5 NDT3-C 17 9.19 13.5 NDT3-C 17 9.19 13.5 NDT3-C 17 9.19 13.5 NDT3-C 17 9.19 13.5 NDT3-D 0.5 12.29 0.5 4.52 0.37 0.09 12.76 1.24 0.25 NDT3-D 1.5 12.75 1.5 1.76 0.14 15.91 1.25 0.34 NDT3-D 3.5 9.93 3.5 0.49 0.05 12.36 1.24 0.25 NDT3-D 4.5 11.86 4.5 11.07 1.25 0.19 NDT3-D 5.5 8.88 5.5 0.02 0.00 10.00 11.48 1.23 0.23 NDT3-D 7.5 9.31 7.5 0.01 0.00 11.48 1.23 0.23 NDT3-D 7.5 9.31 7.5 0.01 0.00 11.48 1.23 0.23 NDT3-D 7.5 9.31 7.5 0.01 0.00 11.48 1.23 0.23 NDT3-D 1.5 11.129 11.5 0.49 0.00 10.73 1.25 1.0 0.80 0.47 NDT3-D 1.5 11.129 11.5 0.49 0.04 9.05 0.80 0.47 NDT3-D 1.5 11.129 11.5 0.49 0.04 0.05 12.35 1.01 0.38 NDT3-D 1.5 9.88 12.5										0.09
NDT3-A 19 - 14.5 0.00 0.00 0.00 0.00 0.00 0.26 NDT3-C 0.5 5.21 0.5 1.68 0.32 4.28 0.82 0.33 NDT3-C 1.5 8.47 1.5 0.08 0.01 6.94 0.82 0.26 NDT3-C 2.5 9.38 2.5 0.06 0.01 0.00 0.00 0.00 0.00 NDT3-C 3.5 5.82 3.5 0.33 0.06 4.79 0.82 0.28 NDT3-C 4.5 5.99 4.5 0.05 0.01 4.88 0.81 0.22 NDT3-C 5.5 6.79 5.5 0.07 0.01 0.00 0.00 0.05 NDT3-C 5.5 6.79 5.5 0.07 0.01 0.00 0.00 0.05 NDT3-C 7.5 7.25 7.5 0.03 0.00 5.66 0.78 0.19 NDT3-C 7.5 7.25 7.5 0.03 0.00 0.00 0.00 0.00 0.01 NDT3-C 8.5 11.10 8.5 0.13 0.01 9.17 0.83 0.19 NDT3-C 9.5 7.24 9.5 0.01 0.00 5.69 0.79 0.22 NDT3-C 11 7.24 10.5 0.04 0.01 5.14 0.71 0.22 NDT3-C 13 6.38 11.5										0.08
NDT3-C										0.00 0.09
NDT3-C										0.09
NDT3-C 2.5 9.38 2.5 0.06 0.01 0.00 0.00 0.00 0.00 NDT3-C 3.5 5.82 3.5 0.33 0.06 4.79 0.82 0.28 NDT3-C 4.5 5.99 4.5 0.05 0.01 4.88 0.81 0.22 NDT3-C 5.5 6.79 5.5 0.07 0.01 0.00 0.00 0.00 0.05 NDT3-C 6.5 7.22 6.5 0.02 0.00 5.66 0.78 0.19 NDT3-C 7.5 7.25 7.5 0.03 0.00 0.00 0.00 0.00 0.01 NDT3-C 8.5 11.10 8.5 0.13 0.01 9.17 0.83 0.19 NDT3-C 9.5 7.24 9.5 0.01 0.00 5.69 0.79 0.22 NDT3-C 11 7.24 10.5 0.04 0.01 5.14 0.71 0.22 NDT3-C 15 7.73 12.5 0.04 0.01 5.14 0.71 0.22 NDT3-C 15 7.73 12.5 0.00 0.04 0.01 5.14 0.71 0.22 NDT3-C 15 7.73 12.5 0.00 0.04 0.01 5.14 0.71 0.22 NDT3-C 15 7.73 12.5 0.0 0.04 0.01 5.14 0.71 0.22 NDT3-C 15 7.73 12.5 0.00 0.00 0.00 0.00 0.00 0.00 0.05 NDT3-D 0.5 12.29 0.5 4.52 0.37 0.00 0.00 0.00 0.05 NDT3-D 1.5 12.75 1.5 1.76 0.14 15.91 1.25 0.34 NDT3-D 2.5 10.26 2.5 0.95 0.09 12.76 1.24 0.25 NDT3-D 3.5 9.93 3.5 0.49 0.05 12.36 1.24 0.25 NDT3-D 4.5 11.86 4.5 -										0.09
NDT3-C										0.00
NDT3-C 4.5 5.99 4.5 0.05 0.01 4.88 0.81 0.22 NDT3-C 5.5 6.79 5.5 0.07 0.01 0.00 0.00 0.05 NDT3-C 6.5 7.22 6.5 0.02 0.00 5.66 0.78 0.19 NDT3-C 7.5 7.25 7.5 0.03 0.00 0.00 0.00 0.00 0.01 NDT3-C 7.5 7.25 7.5 0.03 0.00 0.00 0.00 0.00 0.01 NDT3-C 9.5 7.24 9.5 0.01 0.00 5.69 0.79 0.22 NDT3-C 11 7.24 10.5 0.04 0.01 5.14 0.71 0.22 NDT3-C 13 6.38 11.5										0.09
NDT3-C 5.5 6.79 5.5 0.07 0.01 0.00 0.00 0.05 NDT3-C 6.5 7.22 6.5 0.02 0.00 5.66 0.78 0.19 NDT3-C 7.5 7.25 7.5 0.03 0.00 0.00 0.00 0.00 0.01 NDT3-C 8.5 11.10 8.5 0.13 0.01 9.17 0.83 0.19 NDT3-C 9.5 7.24 9.5 0.01 0.00 5.69 0.79 0.22 NDT3-C 11 7.24 10.5 0.04 0.01 5.14 0.71 0.22 NDT3-C 13 6.38 11.5	NDT3-C	4.5	5.99			0.01	4.88	0.81		0.07
NDT3-C 6.5 7.22 6.5 0.02 0.00 5.66 0.78 0.19 NDT3-C 7.5 7.25 7.5 0.03 0.00 0.00 0.00 0.00 NDT3-C 8.5 11.10 8.5 0.13 0.01 9.17 0.83 0.19 NDT3-C 9.5 7.24 9.5 0.01 0.00 5.69 0.79 0.22 NDT3-C 11 7.24 10.5 0.04 0.01 5.14 0.71 0.22 NDT3-C 13 6.38 11.5										0.02
NDT3-C 8.5				6.5						0.06
NDT3-C 9.5 7.24 9.5 0.01 0.00 5.69 0.79 0.22 NDT3-C 11 7.24 10.5 0.04 0.01 5.14 0.71 0.22 NDT3-C 13 6.38 11.5 -										0.00
NDT3-C 11 7,24 10.5 0.04 0.01 5.14 0.71 0.22 NDT3-C 13 6.38 11.5 -										0.06
NDT3-C 13 6.38 11.5 - <										0.07
NDT3-C 15 7,73 12.5 - <										0.07
NDT3-C 17 9.19 13.5										-
NDT3-D 0.5 12.29 0.5 4.52 0.37 0.00 0.00 0.05 NDT3-D 1.5 1.275 1.5 1.76 0.14 15.91 1.25 0.34 NDT3-D 2.5 10.26 2.5 0.95 0.09 12.76 1.24 0.25 NDT3-D 3.5 9.93 3.5 0.49 0.05 12.36 1.24 0.25 NDT3-D 4.5 11.86 4.5 - - 14.80 1.25 0.22 NDT3-D 5.5 8.88 5.5 - - - 11.07 1.25 0.19 NDT3-D 6.5 10.20 6.5 0.12 0.01 12.62 1.24 0.20 NDT3-D 8.5 8.58 8.5 0.02 0.00 10.73 1.25 0.22 NDT3-D 9.5 9.11 9.5 0.41 0.05 9.95 1.09 0.30 NDT3-D 11 12.19 </td <td></td> <td></td> <td></td> <td></td> <td>-</td> <td>-</td> <td>-</td> <td>-</td> <td>-</td> <td>-</td>					-	-	-	-	-	-
NDT3-D 1.5 12.75 1.5 1.76 0.14 15.91 1.25 0.34 NDT3-D 2.5 10.26 2.5 0.95 0.09 12.76 1.24 0.25 NDT3-D 3.5 9.93 3.5 0.49 0.05 12.36 1.24 0.25 NDT3-D 4.5 11.86 4.5 - 1 14.80 1.25 0.22 NDT3-D 5.5 8.88 5.5 - 1 11.07 1.25 0.19 NDT3-D 6.5 10.20 6.5 0.12 0.01 12.62 1.24 0.20 NDT3-D 7.5 9.31 7.5 0.01 0.00 11.48 1.23 0.23 NDT3-D 8.5 8.58 8.5 0.02 0.00 11.48 1.23 0.23 NDT3-D 8.5 8.58 8.5 0.02 0.00 10.73 1.25 0.22 NDT3-D 9.5 9.11 9.5 0.41 0.05 9.95 1.09 0.30 NDT3-D 11 12.19 10.5 0.26 0.02 12.35 1.01 0.38 NDT3-D 13 11.29 11.5 0.49 0.04 9.05 0.80 0.47 NDT3-D 15 9.88 12.5 - 1 0.49 0.04 9.05 0.80 0.47					452	0.27	0.00	0.00	0.05	0.02
NDT3-D 2.5 10.26 2.5 0.95 0.09 12.76 1.24 0.25 NDT3-D 3.5 9.93 3.5 0.49 0.05 12.36 1.24 0.25 NDT3-D 3.5 9.93 3.5 0.49 0.05 12.36 1.24 0.25 NDT3-D 4.5 11.86 4.5 14.80 1.25 0.22 NDT3-D 5.5 8.88 5.5 110.07 1.25 0.19 NDT3-D 6.5 10.20 6.5 0.12 0.01 12.62 1.24 0.20 NDT3-D 7.5 9.31 7.5 0.01 0.00 11.48 1.23 0.23 NDT3-D 8.5 8.58 8.5 0.02 0.00 10.73 1.25 0.22 NDT3-D 9.5 9.11 9.5 0.41 0.05 9.95 1.09 0.30 NDT3-D 11 12.19 10.5 0.26 0.02 12.35 1.01 0.38 NDT3-D 13 11.29 11.5 0.49 0.04 9.05 0.80 0.47 NDT3-D 15 9.88 12.5										0.02
NDT3-D 3.5 9.93 3.5 0.49 0.05 12.36 1.24 0.25 NDT3-D 4.5 11.86 4.5 - - 14.80 1.25 0.22 NDT3-D 5.5 8.88 5.5 - - 11.07 1.25 0.19 NDT3-D 6.5 10.20 6.5 0.12 0.01 12.62 1.24 0.20 NDT3-D 7.5 9.31 7.5 0.01 0.00 11.48 1.23 0.23 NDT3-D 8.5 8.58 8.5 0.02 0.00 10.73 1.25 0.22 NDT3-D 9.5 9.11 9.5 0.41 0.05 9.95 1.09 0.30 NDT3-D 11 12.19 10.5 0.26 0.02 12.35 1.01 0.38 NDT3-D 13 11.29 11.5 0.49 0.04 9.05 0.80 0.47 NDT3-D 15 9.88 12.5<										0.08
NDT3-D 4.5 11.86 4.5 14.80 1.25 0.22 NDT3-D 5.5 8.88 5.5 - 110.07 1.25 0.19 NDT3-D 6.5 10.20 6.5 0.12 0.01 12.62 1.24 0.20 NDT3-D 7.5 9.31 7.5 0.01 0.00 11.48 1.23 0.23 NDT3-D 8.5 8.58 8.5 0.02 0.00 10.73 1.25 0.22 NDT3-D 9.5 9.11 9.5 0.41 0.05 9.95 1.09 0.30 NDT3-D 11 12.19 10.5 0.26 0.02 12.35 1.01 0.38 NDT3-D 13 11.29 11.5 0.49 0.04 9.05 0.80 0.47 NDT3-D 15 9.88 12.5					0155	0105				0.08
NDT3-D 5.5 8.88 5.5 11.07 1.25 0.19 NDT3-D 6.5 10.20 6.5 0.12 0.01 12.62 1.24 0.20 NDT3-D 7.5 9.31 7.5 0.01 0.00 11.48 1.23 0.23 NDT3-D 8.5 8.58 8.5 0.02 0.00 10.73 1.25 0.22 NDT3-D 9.5 9.11 9.5 0.41 0.05 9.95 1.09 0.30 NDT3-D 11 12.19 10.5 0.26 0.02 12.35 1.01 0.38 NDT3-D 13 11.29 11.5 0.49 0.04 9.05 0.80 0.47 NDT3-D 15 9.88 12.5										0.07
NDT3-D 6.5 10.20 6.5 0.12 0.01 12.62 1.24 0.20 NDT3-D 7.5 9.31 7.5 0.01 0.00 10.73 1.25 0.22 NDT3-D 8.5 8.58 8.5 0.02 0.00 10.73 1.25 0.22 NDT3-D 9.5 9.11 9.5 0.41 0.05 9.95 1.09 0.30 NDT3-D 11 12.19 10.5 0.26 0.02 12.35 1.01 0.38 NDT3-D 13 11.29 11.5 0.49 0.04 9.05 0.80 0.47 NDT3-D 15 9.88 12.5 - <th< td=""><td></td><td></td><td></td><td></td><td></td><td></td><td></td><td></td><td></td><td>0.06</td></th<>										0.06
NDT3-D 7.5 9.31 7.5 0.01 0.00 11.48 1.23 0.23 NDT3-D 8.5 8.58 8.5 0.02 0.00 10.73 1.25 0.22 NDT3-D 9.5 9.11 9.5 0.41 0.05 9.95 1.09 0.30 NDT3-D 11 12.19 10.5 0.26 0.02 12.35 1.01 0.38 NDT3-D 13 11.29 11.5 0.49 0.04 9.05 0.80 0.47 NDT3-D 15 9.88 12.5 - - - - - - -					0.12	0.01				0.07
NDT3-D 9.5 9.11 9.5 0.41 0.05 9.95 1.09 0.30 NDT3-D 11 12.19 10.5 0.26 0.02 12.35 1.01 0.38 NDT3-D 13 11.29 11.5 0.49 0.04 9.05 0.80 0.47 NDT3-D 15 9.88 12.5										0.08
NDT3-D 11 12.19 10.5 0.26 0.02 12.35 1.01 0.38 NDT3-D 13 11.29 11.5 0.49 0.04 9.05 0.80 0.47 NDT3-D 15 9.88 12.5										0.07
NDT3-D 13 11.29 11.5 0.49 0.04 9.05 0.80 0.47 NDT3-D 15 9.88 12.5	NDT3-D	9.5	9.11		0.41	0.05	9.95	1.09	0.30	0.10
NDT3-D 15 9.88 12.5										0.13
					0.49	0.04	9.05	0.80	0.47	0.16
					-	-	-		-	-
	NDT3-D	17	9.14	13.5	-			-	-	-
NDT3-D 19 10.26 14.5	NDT3-D	19	10.26	14.5	-	-	-	-	-	-